POLITECNICO DI MILANO

Corso di Laurea in

Ingegneria Biomedica

MAGNETIC ACTUATED SURGICAL INSTRUMENTATION:

DESIGN OF AN INTERNAL TISSUE RETRACTOR

Relatore: Elena De Momi PhD

Correlatori esteri: Pietro Valdastri Prof., Vanderbilt University, TN. USA
Christian Di Natali PhD, Vanderbilt University, TN. USA
Beccani Marco PhD, Vanderbilt University, TN. USA

Tesi di Laurea di:

Nicolò Garbin matricola 781285

Anno Accademico 2012 - 2013.

Index

List of Figures

effector. At the end effector tip a wired grasper is used for retracting purpose. The retracted weight is unloaded by the anchoring unit.

Figure 2.2: Schematic 2D model of a actuation unit. The EPM having magnetization M_D described by the angular displacement θ_D induce torque on the IPM having magnetization M_d having θ_d as angular displacement.

Figure 2.3: Comsol Gui with highlighted model builder's steps, that lead to the implementation of the simulation.

Figure 2.4: bench test utilized for dynamically characterize and study the selected actuation unit PMs. A motor mounted on a vertical slider is connected to the EPM. The IPM is connected to a dynamometer having the same EPM axis of rotation. Two hall effect sensors (P15A) are used to determine the angular position (θ_D and θ_d)of both the PM.

Figure 2.5: purchased actuation unit couple of EPM and IPM (K&J Magnetics, Jaminson U.S).

Figure 2.6: T_{max} at varying the separation distance. red dots: simulation data and in blue their exponential regression.

Figure 2.7: a) result of the dynamical study of torque transferring at varying the separation distance. In blue the bench test results, in red the static simulation regression line. b) result of the dynamical study of the torque transferring at varying the actuation unit velocity. Different color correspond constant separation distance.

Figure 2.8: a) 3D rendering of an epicyclical gear with a planetary arrangement that show the position of sun (S), 4 planets (P) and annular gear (A). b) epicyclical gear where the carrier is highlighted to show how the planets mate with it. c) sense of rotation of each components of a planetary gear system when the annular gear motion is fixed.

Figure 2.9: Pro/e snapshot of the parametric model of a spur gear

Figure 2.10: bench test used for calculating the efficiency of the designed planetary gearhead. An EC motor deliver input speed and input torque (τ_{in} and ω_{in}) to the planetary gearhead system, the dynamometer represent the output load τ_{out}. Connected to the dynamometer shaft a PM is used to measure the output velocity ω_{out}.

List of Table

Sommario

INTRODUZIONE

La laparoscopia è una tecnica chirurgica che prevede l'inserimento di strumenti chirurgici nell'addome del paziente attraverso piccole incisioni. L'addome viene insufflato e tramite una videocamera inserita attraverso una delle incisioni, il chirurgo può vedere e manipolare gli strumenti chirurgici all'interno dell'addome in maniera mini invasiva. Un elevato numero di incisioni però aumenta il rischio di infezioni, quindi convalescenza per il paziente e costi aggiuntivi per l'ospedale. L'invasività della laparoscopia, considerando i costi e i tempi medi richiesti per trattare un'infezione chirurgica, è stata infatti quantificata e supera i 100 milioni di dollari annui negli USA.

Per poter effettuare operazioni attraverso una singola incisione, recentemente sono stati proposti complessi sistemi micro robotici che riproducono in scala ridotta le braccia del chirurgo all'interno della cavità addominale. Motori a bordo o sistemi a cavi con attuatori all'esterno del corpo pero non garantiscono un'elevata performance dal chirurgo. Lo spazio di lavoro è limitato e le prestazioni in termini di potenza meccanica disponibile sull'end effector dello strumento non sono sufficienti.

Un nuovo approccio che sfrutta le interazioni dei campi magnetici di magneti permanenti può pero permettere lo sviluppo di strumenti chirurgici disaccoppiati: un dispositivo che entrata da una singola incisione può essere mosso e attuato da un controllore esterno magneticamente. Unità di ancoraggio e di attuazione, accoppiate magneticamente a cavallo dello spessore addominale, garantisco agli strumenti cosi definiti uno spazio di lavoro aumentato, una maggiore potenza trasferita all'interno della cavità addominale e l'utilizzo di tecniche di sterilizzazione meno costose. Con questo tipo di tecnologia un retrattore interno di tessuti è stato progettato, fabbricato e testato.

Le caratteristiche tecniche di un retrattore interno di tessuti per laparoscopia da un punto di vista robotico, sono la presenza di un grado di liberta capace di controllare il grado di retrazione imposto e una forza esercitata dall'end effector di almeno 6 N.

MATERIALI E METODI

Il funzionamento dello strumento è determinato dalla quantità di potenza trasferita, quindi convertita per retrarre tessuti (unita di attuazione), e dalla forza di attrazione in grado di supportare il peso retratto (unita di ancoraggio).

Il treno meccanico, progettato per essere contenuto in uno strumento di 12 mm di diametro, utilizzato per convertire la potenza trasmessa e quindi effettuare la retrazione è composto da:

- Una trasmissione magnetica (unita di attuazione) in cui un magnete permanente, contenuto nel controllore esterno, trasferisce coppia meccanica in maniera wireless a un magnete interno, inserito nel retrattore. Il magnete interno può quindi essere considerato come un motore a bordo dello strumento.
- Un riduttore epicicloidale di dimensioni ridotte e elevato rapporto di trasmissione che converte la potenza meccanica aumentando la coppia in uscita e diminuendo la velocità di rotazione.
- Una vite senza fine che, connessa a un sistema biella a manovella decentrato, permette il controllo della posizione di una leva al cui termine è legata una clip utilizzata per afferrare il tessuto da retrarre.

La capacita di sostegno è invece determinata da come le forze di attrazione, di entrambe le unita magnetiche, sono posizionate all'interno dello strumento e quindi che momento (generato dalla forza del peso retratto) sono in grado di sostenere.

Sia la potenza trasferita che la forza di attrazione delle due unità, decadono esponenzialmente al crescere della distanza tra i magneti interni e quelli esterni.

Quindi il parametro più importante intorno a cui è stata fatta ruotare la progettazione e scelta dei materiali più idonei, è stata la distanza che intercorre tra il retrattore inserto e il controllore esterno (i.e. spessore della parete addominale).

Simulazioni ad elementi finiti in Comsol sono state utilizzate per il calcolo della coppia trasmissibile e della forza di attrazione che due magneti sono in grado di esercitare al variare della distanza. Analizzando i risultati ottenuti sono quindi stati scelti i magneti da utilizzare. Banchi prova dedicati hanno quindi permesso la validazione delle simulazioni grazie a, da una parte, lo studio del comportamento dinamico della trasmissione magnetica, dall'altra, lo sviluppo di un modello per la predizione del peso sostenibile.

Le componenti meccaniche sono invece state progettate in Pro Engineering per soddisfare i requisiti tecnici di dimensioni. Sono quindi state fabbricate e caratterizzate tramite banchi prova specifici e studi cinematici in Matlab.

RISULTATI

Dai risultati intermedi ottenuti dallo studio di ciascun componente, è stato possibile riassumere il funzionamento del retrattore per diversi spessori addominali in termini di peso che può essere stabilmente retratto e sostenuto. In figura 0.1 è riportato in nero il peso che il retrattore è in grado di sostenere, in blu il peso che può essere retratto.

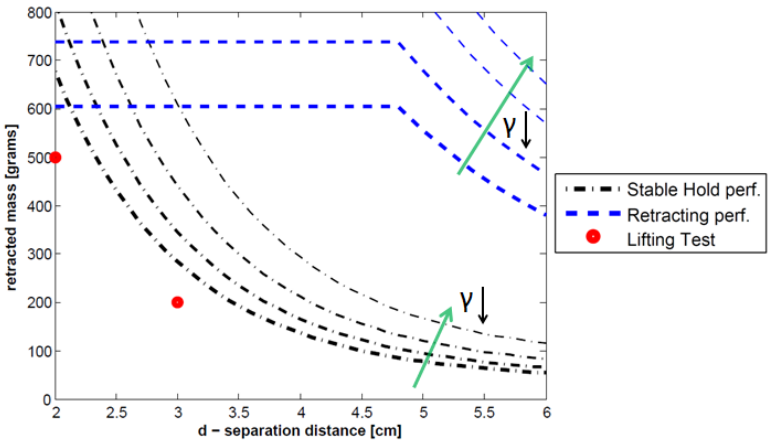

Figure 0.1: performance dello strumento al variare dello spessore addominale. In nero il sostegno offerto dalle forze di attrazione, in nero la massa che può essere retratta dal treno meccanico. Entrambe le performance aumentano con la chiusura della leva di retrazione (angolo γ), garantendo un funzionamento sicuro del dispositivo.

Due test conclusivi in cui masse note sono state sollevate simulando valori di spessore addominale noti, hanno quindi verificato il funzionamento del dispositivo. Addizionali test ex vivo hanno invece qualitativamente analizzato la soluzione di retrazione proposta. La retrazione di un fegato di maiale ha infine mostrato come lo strumento, aderendo alla parete addominale, permette di mostrare i tessuti sottostanti garantendo un ottima visibilità e minimo ingombro dello spazio di lavoro.

DISCUSSIONE

Il funzionamento del retrattore risulta stabile e affidabile in quanto le prestazioni aumentano all'aumentare dello spostamento imposto (angolo γ della leva), figura 0.1. Il retrattore cosi sviluppato può entrare attraverso trocar standard, essere mosso ed attuato perfino all'interno di pazienti obesi (parete addominale media 4 cm). Il peso che può essere retratto risulta rilevante (> 500 grammi) e maggiore rispetto al peso che può essere sostenuto. L'unita di ancoraggio può quindi essere ridimensionata grazie alla modularità del sistema e permettere un efficace retrazione anche in pazienti obesi.

Il retrattore sviluppato è il primo strumento chirurgico basato su attuazione e ancoraggio magnetico.

Abstract

INTRODUCTION

Laparoscopy is a surgical technique performed with the insertion of different surgical instrumentations through small incisions in the patient abdominal cavity. The abdomen is insufflated and thanks to a vision module, inserted thought one of the incisions, the surgeon can see and manipulate the surgical instruments, operating in a mini invasive way. However a high number of incisions increase the infection risk and thus convalescence for the patients and costs for the hospital. Considering cost and time requests for treating a surgical infection, the invasiveness of laparoscopy had been quantified exceeding $ 100 per year in the USA.

Surgical robotic manipulators that enters the abdominal cavity through a single incision had been recently proposed as solution to this problem. Unfortunately the drawbacks of this technology cannot guarantee a clinical use: the workspace is limited and the performance of the robotic arms are insufficient (i.e. the power that can be inserted in the abdominal cavity though small incision is not enough).

A new approach that exploit the magnetic fields of permanent magnets allow the development of surgical instrumentation decoupled: an insertable device that enter from a single incision, can be maneuvered and actuated by an external controller. A magnetic anchoring unit and an actuation one, coupled across the abdominal thickness and embedded both in the internal device and the outside the body coupler, offer an increased workspace, a higher mechanical power that can be transferred wirelessly and cheaper sterilization methods.

With this approach, an internal tissue retractor had been designed, fabricated and tested.

A surgical retractor, to be effective, has to enter from a standard incision, be able to generate a force of 6 N and control the imposed displacement keeping it stable.

MATERIALS AND METHODS

The device performance is determined by the quantity of power that can be transferred, then converted to retract, and by the attraction forces able to sustain the retracted weight.

The mechanical train designed to convert the transmitted power and to actuated a retracting end effector, is composed by:

- A magnetic spur gear transmission (actuation unit) where the external permanent magnet, embedded in the external controller, transfer torque wirelessly to the internal one. This, embedded in the retractor, can be considered as an on board motor.
- A planetary gearhead with small dimensions that converts the mechanical power increasing the output torque and decreasing the output speed.
- A power screw that, connected to an offset crank mechanism, controls the angular displacement of a lever at which tip, a wired clip is used to clutch the target tissue.

The support capability is instead determine by the attraction forces of both the magnetic units and how they are placed inside the instrument. Their position, in fact, determine which is the maximum momentum (generated by the retracted weight force) that can be stable hold.

Both power transmission and attraction force of the two units, decrease exponentially at the increase of the separation distance between the internal and external magnets. Thus, the abdominal thickness had been considered the main design parameter.

FEM simulation in Comsol Multiphysics had been used to calculate the transmittable torque and the attraction forces that two permanent magnets are able to exert on each other, at varying the separation distance. From the obtained results, appropriate permanent magnets had been purchased. With the use of the specific bench test it had been possible to determine the dynamic of the actuation unit and develop a model that can predict the weight that can be hold.

The mechanical components had instead been first designed in Pro Engineering to satisfy the dimension limitations, then fabricated and characterized with specific bench tests and kinematic study in Matlab.

RESULTS

Thanks to the components characterization it had been possible to summarize the device functioning at with different abdominal thickness, figure 0.1. The weight that the device is able to stable hold due to attraction forces is represented in black, while in blue is the weight that the mechanical train can retract.

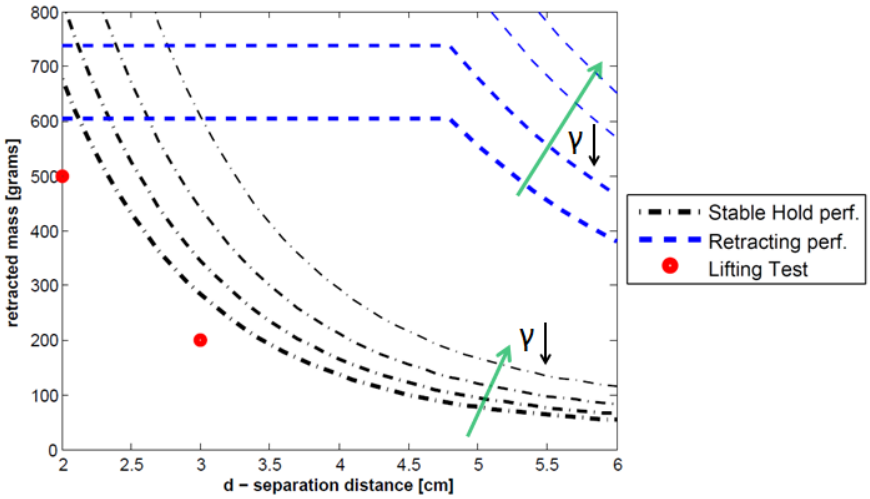

Figure 0.2: device performance at different simulated abdominal wall thicknesses. In back the stable hold performance provide information about the device unload capacity, in black the retract performance measures the equivalent weight that can be lifted by the end effector. Both the performance increases with the lever closure, allowing a secure device functioning.

Two conclusive test (red dots in figure 0.1) where known masses had been retracted at simulated abdominal thickness, validates the device functioning. Additional ex vivo tests had instead been used to qualitatively describe the proposed retracting solution. A pig liver retraction demonstrate how the designed instruments, adherent to the abdominal cavity, shows hidden tissues and guarantees good visibility and minimum encumbrance of the workspace.

DISCUSSION

The designed retractor functioning results stable and reliable. The performances, in fact, increase with the increase of the imposed displacement (retracting lever angle γ), figure 0.1. The retractor can enter though a standard trocar port even inside obese patients (average abdominal thickness 4 cm).

The weight that can be retracted is considerable (> 600 grams) and higher than the one that can be hold. The anchoring unit should be re sized thanks to the modularity of the system. The proposed device is the first magnetically actuated and anchored surgical device.

1 INTRODUCTION

1.1 CLINICAL SCENARIO

Abdominal surgeries are commonly performed with laparoscopic surgery (LPS). This surgical techniques consists in the insertion of different surgical devices in the patient abdominal cavity through small incision ports [1]. Standard trocar with dimensions that range from 0.5 cm to 1.2 cm allow surgeons to reach the internal organs in a mini invasive way, figure 1.1.

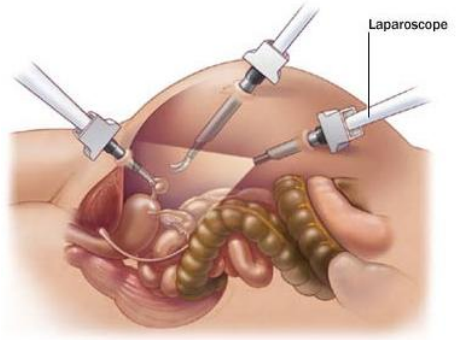

Figure 1.1: In traditional multi-port laparoscopic surgery at least three incisions are created in the patient's abdomen for camera and surgical instrument access. Air insufflations creates the space required for the instruments to move.

LPS, compared to traditional open surgery, offers advantages for the patients in terms of faster postoperative recovery, reduced pain, fewer hernias, and better cosmetic outcome [2].

The abdominal cavity is insufflated with the use of carbon dioxide (CO2) so that the surgical workspace is enlarged and the endoscopic vision module offers a better visibility.

Long shaft surgical instruments are inserted and controlled by the surgeon with real time visual feedback thanks to a vision module inserted in the abdominal cavity. Their maneuverability and triangulation, intended as the capacity to replicate the surgeons hands and view inside the abdominal cavity, depends on

the entry port location. The number of incisions required in laparoscopic surgeries varies from three to six, depending on the complexity of the operation and the required devices. A vision module, surgical laser, surgical manipulator and internal tissue retractor are utilized in more than 2 million laparoscopic surgery performed in the United States every year.

However the infection rate can be related to the number of incisions and their dimensions. Considering that $10,500 [3] and 4 additional days of hospitalization are the typical costs of surgical site infections and that infection incidence is 0.5% on a single incision, the invasiveness of traditional LPS had been quantified exceeding $ 100 million per year in the USA [4]. Thus a critical surgical challenge is reducing the invasiveness by minimizing the number of incisions and their size.

Different surgical approached had been proposed and the most promising one are Laparoendoscopic Single Site (LESS) surgery [5] and Natural Orifice Transluminal Endoscopic Surgery (NOTES) [6].

LESS surgery consists in the use of a single multiport access (2.5 cm – 3 cm diameter) placed in the patient navel [7]. The multiport allows the insertion of multiple devices from in the same entry port but their maneuverability in even more complicated and the triangulation very poor. To overcome this limitation angulated shaft device had been studied so that reproduce the surgeons arm inside the abdominal cavity, figure 1.2.

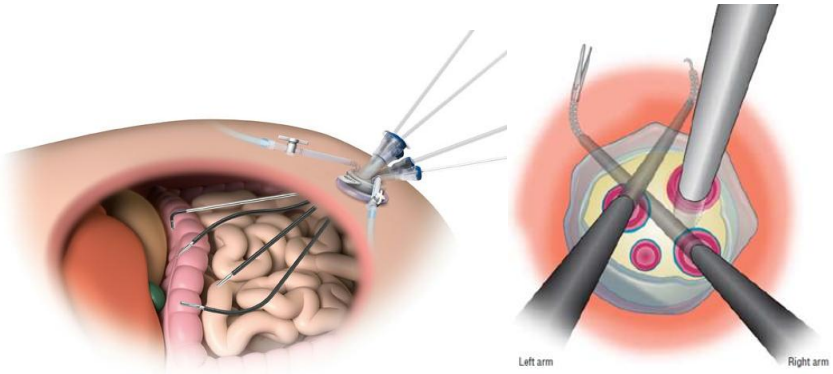

Figure 1.2 In LESS surgery a single multiport placed in the patient navel allow the insertion of multiple surgical device through a single incision of 2,5-3 cm diameter.

Because of the geometry of the problem the right and left instruments are controlled by the opposite surgeons hands and it had been demonstrated that surgeons' performance is lower than with a tradition laparoscopic approach [8].

NOTES approach aims is to reach the abdominal cavity entering from natural orifice such as vagina, anus or mouth. An internal incision, that have lower infection risk, allows steerable surgical device, with the same technology of traditional endoscope, to reach the abdominal cavity, figure 1.3.

Figure 1.3: In NOTES surgery, natural orifice can be used to reach the abdominal cavity with steerable device that integrates in its tip a grasper, a tissue cutter-sampler and a stereoscopic camera.

Surgical devices that are steered from their handle and integrates surgical manipulators and the vision module at their tip [9], cannot guarantee good dexterity and have an more reduced visibility and triangulation.

To overcome this limitations, since the DaVinci (Intuitive Surgical, Sunnydale California, USA) robotic platform is revolutionizing the surgical scenario [10], robotic devices for LESS and NOTES surgeries had been recently developed [11][12]. Robotic arms with on board micro motors can enter through a small incision the abdominal cavity and reproduce very precise movements while controlled directly from the outside the body with haptics platform [13]. The constrain given by the entry port dimensions limits the power that can be placed on board while the poor triangulation given by insertable robotic arms cannot perform all the surgical tasks.

1.2 LOCAL MAGNETI ACTUATION (LMA)

A completely new approach, named Local Magnetic Actuation (LMA), for developing surgical assisted instruments that can overcomes these limitations had been proposed by Di Natali et al. [14][15][16] and consists in the interaction of magnetic field of permanent magnets for positioning and actuating surgical devices. Magnetic coupling is indeed one of the few physical phenomena able in transmitting actuation forces across a physical barrier: surgical devices that embed permanent magnets can be mobile and a separate incision is no longer needed since they can simply enter the abdominal cavity and be controlled with an external controller.

Each LMA-based device is composed by at least one anchoring unit, plus and actuation unit per independent DoF. The anchoring unit is composed of an external and an internal permanent magnet and it function is to support the instrument during surgery. The actuation unit is composed by an external

driving and an internal driven permanent magnet. The driving magnet, connected to a motor that can be actuated independently, causes the actuation of the respective driven magnets, coupled across the abdominal wall. The driven magnet is use to actuate, through a mechanism one DoF of the end effector, figure 1.4.

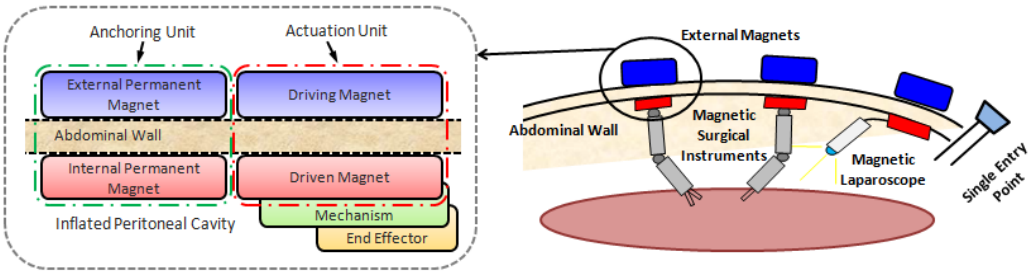

Figure 1.4: Concept definition and schematic representation of LMA based surgical instruments that can enter the abdominal wall and be controlled and actuated with the used of magnetic fields of permanent magnets that couple across the abdominal wall thickness.

1.3 AIM OF THE WORK

In order to investigate the feasibility of the proposed approach and present a first LMA based device the aim of this work are:

1) Design and LMA based internal tissue retractor for laparoscopic surgery able to anchor (being hold in place) and transfer wireless mechanical power across the abdominal wall.

1.4 TISSUE RETRACTORS

Proper tissue retraction is fundamental in abdominal surgery. The gallbladder and the stomach, for example, lay underneath the right lobe of the liver and for a better visibility and exposure to the surgical workspace, liver retraction is fundamental. In LPS, retraction is performed with the use of long shaft retractors that enters the abdominal cavity through a dedicated port or with insertable grasping device that are used to attach in an invasive way the target tissue to the abdominal wall.

Long shaft retractor require a dedicated operator or a dedicated robotic arm for robotic surgery, to maneuver and hold the retracted tissue.

This type of retractors, such as Endo Retract II (Convidien MA, USA) [17] depicted in figure 1.5, can reach a target with limited configurations due to the dependence on the entry port location.

Figure 1.5: Commercially available internal tissue retractor used in LPS. Condivien Endo Retract II. (10 mm diameter) [17].

This type of continuous retractor disturbs the surgeons view at the point of interest and encumber the surgical workspace complicating the surgeons actions. Retractors such as the commercial product EndoLift (Virtual Port, Caesarea Israel) [18], are instead intended to enter the abdominal wall through 5 mm incisions and anchor the target tissue to the peritoneal tissue with the use of invasive hooks mechanism. Both the tissue and the peritoneal cavity is perforated several time during the operation, increasing patient post operative pain.

With the aim of eliminating these problems and decrease the number of incision ports, magnetic anchored systems had been investigated.

New generation of permanent magnets (PM) able of entering the abdominal cavity through standard trocar port can generate, due to the interaction with an external PM, high attraction forces that can be used to retract internal tissues.
With this approach, internal permanent magnet can enter the abdominal workspace through an incision that is then used for other instrumentation insertion. Moreover, the dedicated operator issue is solved by the stable anchoring with the external permanent magnet and the workspace is left free since the internal PM is positioned on the workspace edges.
Magnetic retracting solutions that exploit the attraction forces between internal and external permanent magnets had been proposed and tested.
Padilla [19](figure 1.6), Cho [20] and Kume [21] designed and investigate a similar retraction solution. The internal PM, sutured-grasped to the target tissue, is attracted by the external PM and is able generate a displacement that is function of the magnetic interaction between the selected PMs and of the target weight.

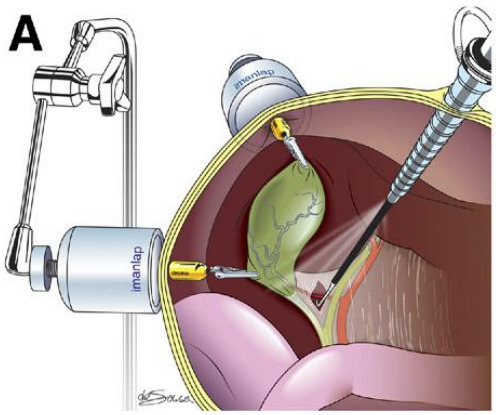

Figure 1.6. Padilla proposes the use of PM in traditional LPS to perform gallbladder resection. The internal PM is grasped to the target and generate a displacement due to the interaction with the external PM. [19]

The maneuverability for surgeons is increased and once the tissue is removed, it can be taken out the patient body with the internal permanent magnet directly attach to it.
Nevertheless this approach cannot control the retraction grade**.** The tissue is either displaced depending on the attraction force, or is not displaced at all.
A degree of freedom that control an actuation system is thus necessary in a retracting system.

To actuated an insertable device the investigated solution, so far, had been either with micro motors on board or with the relative displacement of multiple internal permanent magnets device.
Tortora [22], in particular, had designed a magnetically anchored articulated arm with a grasper like end effector. Two micro motor (4-mm diameter brushless motors by Namiki Jewels, Tokyo, Japan) embedded inside the robotic device control two degrees of freedom: the arm angular displacement and the end effector grasper closure utilized to clutch the tissue. Due to the limited size the power and thus retracting capacity of the proposed mechanism are very poor. A maximum pulling force of 1.53 N is reported.
Canes [23] designed a magnetically anchored tissue retractor that embed a DC motor connected to a drum. The motor rotation is used to wound and unwound a tethered grasper use to clutch the tissue that has to be retracted. No specification are provided neither further investigation on the proposed design are yet available.
Park and Zelter [24] [25] had instead designed a retractor based on permanent magnets only. A lever like retractor opens and closes depending on the relative position of two internal PM placed at the device extremities figure 1.7.

Figure 1.7: Park magnetic tissue retractor. A mechanism control the angular displacement of a retracting lever due to the translation of permanent magnets placed at the device extremity. [23]

The proposed design integrate a fan-like end effector to improve the device stability and retract a bigger portion of tissues. Specification in term of the device performance are not discussed and thus also this approach cannot be considered clinically accepted.

Retractors are surgical devices with high force requirements but without speed limitation or requests [26-28].
Due to the dimension constrain of standard laparoscopic incision, device with on board motors have very low performance in term of retracting force. Moreover motorized device requires low temperature sterilization method like ethylene oxide that is pricy and requires a resting time for the total evaporation of the chemical compound.

1.5 Laparoscopic Retractor based on Local Magnetic Actuation (LapR_LMA)

The proposed device is an insertable tissue retractor for laparoscopic surgery that exploit the magnetic field of PMs with two different approaches with the LMA approach described in section 1.2.
An **anchoring unit** guarantee device motion inside the surgical workspace, positioning and unload of the retracted weight. An **actuation unit** composed by

a driving outside the body PM and an internal driven PM, is instead responsible of wireless transfer of power on board. A mechanical train, than fit inside a 12 mm diameter device, connected to the internal driven PM, actuate an end effector able to retract internal organs, Figure 1.8.

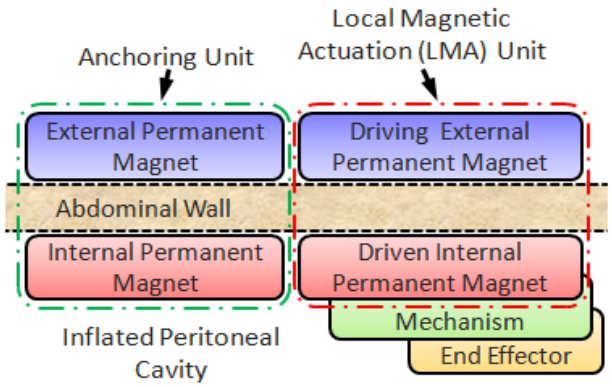

Figure 1.8: LMA based surgical device concept definition to schematically represent a tissue retractor main components.

Both the unit are composed by two PM, an external one (EPM) and an internal one (IPM) that couple across the abdominal wall. The unit performances are determined by the two PM interaction and this definition allow to split in two the dimensioning problem: the IPMs has to be small enough to fit the insertable device dimension constrains, while the EPMs do not have size limitation. The actuation unit can transfer on board, an amount of power much higher than EC motors with the same size of the IPM have. Any internal organ can be retracted and supported by the anchoring unit.

In the following section the clinical requirements are analyzed and quantified in technical requirements that have been used to constrain the design of the LapR_LMA. Chapter 2 first schematically introduces the device components and the retraction solution proposed, then the definition-realization-testing of

each of them is listed with a IMRAD (Introduction, Material and Method, Results And Discussion) format.

Chapter 3 presents the realized LarR_LMA describing its performances and shows evaluation tests that had been performed.

Chapter 4 discuss the obtained final results while chapter 5 announces the future directions and possible improvement.

1.6. CLINICAL REQUIREMENTS (CR)

In order to develop a magnetically actuated tissue retractor a previous outlook of which are the clinical requirements (CR) is necessary so that the design development is constrained. Figure 1.9 shows a representation of the surgical environment and highlight the clinical requirements, that had been taken in consideration which are subsequently described.

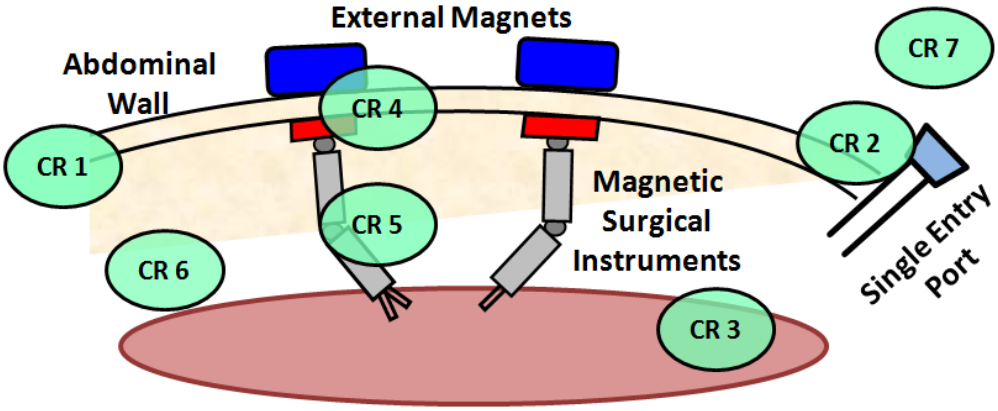

Figure 1.9: CRs investigation for developing the laparoscopic tissue retractor based on LMA.

- **CR1**: ABDOMINAL WALL THICKNESS

The proposed device is actuated and positioned thanks to the interaction between and EPM and an IPM across the abdominal wall. The separation

distance between the PMs is thus a critical parameter and must be quantify taking in consideration the majority of the patients. Obese patients (Body Mass Index > 30kg/m^2) abdominal thickness had been investigated by Best [29] who reported that it can be considered no thicker than 4 cm.

- CR2: INCISION DIAMETER, ENTRY PORT DIMENSION

The dimension of the incisions used in traditional LPS, depends on the instruments that is inserted through. Standard trocar diameter ranges from 0.5 cm to 1.2 cm for the vision module [30]. Hence the insertable device diameter has to not exceed 12 mm in diameter to enter the abdominal cavity. The port is used to introduce the device and is then left free for other instrumentations.

- CR3: WEIGHT OF THE RETRACTED TISSUE.

The heaviest abdominal organ is the liver and it had been measured to weights around 1.561 Kg [31]. Since it is composed by two lobes and at maximum one lobe is retracted, a target weight of 750 grams is taken in considered as the maximal weight the designed system must be able to retract and support.

- CR4: MAGNETIC COUPLING HISTOLOGICAL DAMAGE

New generation of permanent magnets are very powerful and can generate potentially dangerous pressure stresses on the abdominal wall. Magnetic coupling histological damage had been investigated by Best et al. [32] and a pressure of 46.7 KPa had been reported to be well tolerated in porcine model. Hence the magnetic units must be designed to generate compression stresses lower than 46.7 KPa.

- CR5: DoF OF A SURGICAL RETRACTOR

Controlling the grade of lifting of the retracted tissue requires one Degree of Freedom (DoF) only. In term of actuation force and velocity, the degree of freedom demands high force (6N) but no velocity constrain [26-28].

- CR6: WORKSPACE

Laparoendoscopic procedures are performed with CO_2 insufflations of the abdominal cavity so that the workspace for surgeon is increased. The dimensions of the workspace, hadn't be modeled or geometrically described yet but Piccigallo et al. [33] in developing a bimanual robotic platform for LESS surgery had reported a maximum distance between the umbilical port and the further point of intervention of 275 mm. The device has to be reasonably small and without sharp edges that can jeopardize the patient safety. The device should also be able to explore the workspace, moving inside the abdominal cavity to reach the best configuration for retracting the interest organ without interfering with other instrumentations.

- CR7: STERLIZIATION

Sterilization is a fundamental procedure all the surgical devices have to undergo. Insertable surgical device with embedded motor and electronics requires low temperature methods as ethylene oxide that is expensive and requires recovery time. Commercially available PM can instead maintain their magnetic properties up to 200° C and can undergo high temperature sterilization in autoclave. Compared to ethylene oxide, autoclave offers cheaper and faster results.

2 DEVELOPMENT OF LapR_LMA

2.0 PRINCIPE OF OPERATION

LapR_LMA is a surgical device composed by two components: an **external handler** and an **insertable device** designed for retracting purpose. The two components are magnetically connected though the abdominal wall thanks the magnetic field interaction of PMs, figure 2.1.

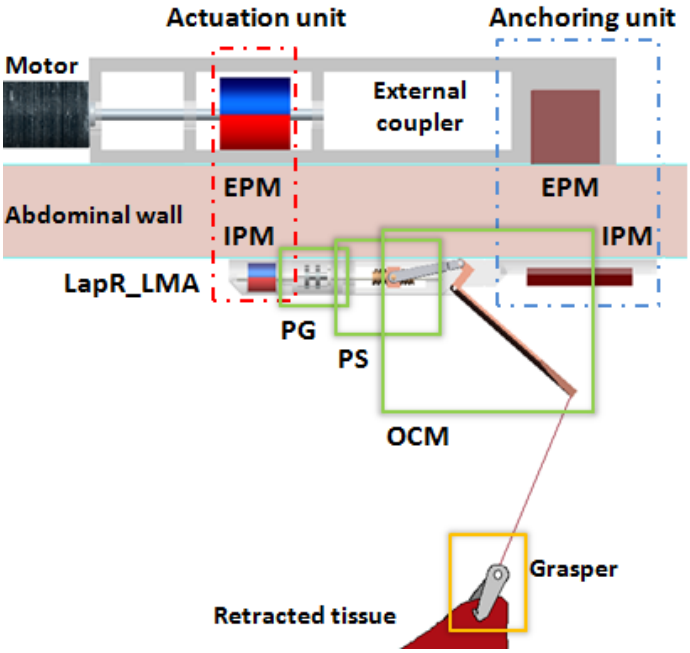

Figure 2.1: schematic representation of the proposed magnetic actuated tissue retractor. Actuation unit transmit wireless power to the IPM connected to a custom made mechanical gear train. A planetary gearhead increase the torque transmitted to a power screw that designed to mate with an crank mechanism actuates a retracting lever end effector. At the end effector tip a wired grasper is used for retracting purpose. The retracted weight is unloaded by the anchoring unit.

Magnetism is exploited with two different approaches: the positioning and unload of the retracted weight is entrusted to an **anchoring unit** where the EPM generate attraction forces on the correspondent IPM; wireless power transmission on board to the untethered device is instead guaranteed by the

actuation unit. The rotation of the actuation unit EPM is corresponded with a synchronous rotation of the respective IPM that can be considered as an equivalent on board motor.

A mechanical train fits the insertable device dimension and had been ad hoc designed and fabricated. A **planetary gearhead** converts the input power reducing the output speed and increasing the output torque and is connected to a mechanical actuation system composed by a **power screw** properly designed to mate with a **crank** mechanism that include a **retracting lever** end effector. A **grasper** wired to the lever tip is used for clutching the **retracted tissue**. Hence the displacement that the proposed retraction solution can generate depends on the retracting lever length and its angular position, figure 2.1.

With the proposed mechanical train solution, high efficiency components that can fit inside a 12 mm diameter, provide almost absent backslash, high speed ratio, non back drivability and precise motion control. Thanks to specific bench tests, each component had been mechanically characterized and a mechanical transfer function, of the proposed train, built. Knowing the input power coming from the Actuation Unit is possible to predict the weight that can be retracted. On the other hand, knowing the attraction forces is possible to predict the weight that can be supported by the device thanks to a structural model.

Hence the device functioning can quantified allowing the used to know beforehand if eventual failure occurs due to insufficient actuation power or attraction forces.

2.1 ACTUATION UNIT

2.1.1 ACTUATION UNIT - INTRODUCTION

Technical requirements

The propose actuation unit must ensure power transmission in a range of distances (abdominal thickness value) that can be applied to the majority of the patients. Wireless power transferring has to be present up to 4 cm (CR 1).

The IPM dimensions have to be chosen so that it can fit inside a 12 mm diameter device (CR2). The EPM dimensions instead do not have dimensions constrains. The magnetization of the selected PM have to resist autoclave sterilization (CR7).

Description

The actuation unit is composed of two ring shaped permanent magnets diametrically magnetized constrained to rotate about their respective axes. The magnets are magnetically coupled and when one magnet rotated it imparts torque on the other causing it to rotate in a synchronous fashion. This magnetic coupling can be mechanically compared to coupling spur gears where the gear ratio of the system depends on the magnetic poles presents on each magnets and not on the number of teeth as for a spur gear transmission system.

The EPM can be intended as the driver magnets, while the IPM as the driven one. In the proposed formulation (figure 2.2) M_D and M_d for the EPM and the IPM magnet respectively, represent the magnetization vector. While the two magnets are assumed having a single dipole (thus gear ratio of the system equals to 1) the angular coordinates θ_D and θ_d as the angular coordinates of M_D and M_d can be defined. The angular displacement of the actuation unit is denoted with $\Delta\theta = \theta_D - \theta_d$.

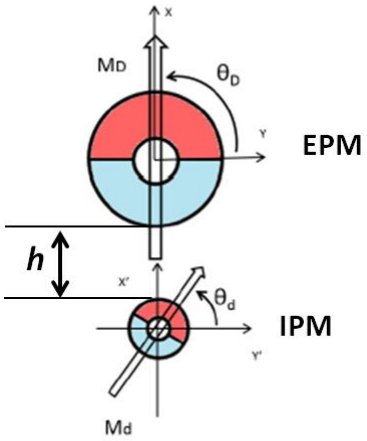

Figure 2.2: Schematic 2D model of a actuation unit. The EPM having magnetization M_D described by the angular displacement θ_D induce torque on the IPM having magnetization M_d having θ_d as angular displacement.

An important assumption of the proposed model is that the two magnets are lying on two parallel axes, spaced by a separation distance h measured with respect of the two facing surfaces.

This magnetic conformation allow not only the generation of attraction forces on the PMs but also torque induction. The torque transmitted across a magnetic gear coupling in fact, is no longer constant with $\Delta\vartheta$ and can be described by a nonlinear trigonometric function, equation 1:

$$Tc\ (h, \Delta\vartheta) = Tmax(h)\ \cdot \sin(\vartheta_D - \ \vartheta_d) = Tmax(h)\ \cdot \sin(\Delta\vartheta)\ \ (1)$$

where T_{max} is the maximum torque that can be transmitted over the magnetic coupling. The value of T_{max} depends on the volume and magnetization intensity (M_D and M_d) of the magnets and on their separation distance, h.

A maximum value of T_c, for a given couple of PM at a certain distance, is thus achieved when the displacement angle $\Delta\vartheta$ is equals to 90°.

Static and dynamical approaches are required to:

- characterize and determine the value of T_{max} at varying the separation distance;
- describe the dynamical behavior of the actuation unit and obtain a transmittable power efficiency, with respect of the static theoretical T_{max}, as a function of angular velocity and separation distance.

In order to statically quantify the transmittable torque and choose EPM and IPM dimensions and magnetization, a method to evaluate the static torque function at varying their separation distance (h) has to be chosen.
A bench test that replicate the model described in figure 2.2 is instead required to dynamically characterized the actuation unit and described the efficiency of the proposed actuation across clinical relevant separation distances.

2.1.2 ACTUATION UNIT - MATERIAL AND METHODS

Static Analysis

The PM analysis is performed with the magnetostatic theory that derives from a review of the Maxwell's equations. The differential form of the Maxwell's equation uncoupled is expressed by equations 2 and 3 while the constitutive relation is showed in equation 4 [34]:

$$\nabla \times H = J \qquad (2)$$

$$\nabla \cdot B = 0 \qquad (3)$$

$$B = \mu_0(H + M) \qquad (4)$$

Where J is the free current, H is the magnetic field intensity, B magnetic flux density, M magnetization vector field and μ_0 the permeability of the free space ($4\pi\times10^{-7}$ H/m).

Equation 2 is the Ampere's circuital law, which states that the circulation of the magnetic field intensity around any closed path is equal to the free current flowing through the surface bounded by the path.
Equation 3 states that the total outward flux of the B-field over a closed surface is zero, thus there are no isolated sources or sinks of magnetic field.

Torque and attraction force acting on PM subject to an extern magnetic field following this formulation can founded with two different approaches: The current model and the charge model.

The first assume the magnet to be a distribution of equivalent volume and surface current densities, J_m and j_m respectively. These currents are used as source term of the magnetostatic field equations.
The magnetic field of a PM can be obtained following equation 5:

$$B(x) = \frac{\mu_0}{4\pi}\int_V J_m(x') \times \frac{(x-x')}{|x-x'|^3}\, dv + \frac{\mu_0}{4\pi}\oint_S j_m(x') \times \frac{(x-x')}{|x-x'|^3}\, ds \quad (5)$$

While force (F) and torque (T) that a permanent magnet is subjected to due to an external magnetic field (B_{ext}) can be calculated with equation 6 and 7 [34]:

$$F = \int_V J_m \times B_{ext}\, dv + \oint_S j_m \times B_{ext}\, ds \qquad (6)$$

$$T = \int_V r \times (J_m \times B_{ext})\, dv + \oint_S r \times (j_m \times B_{ext})\, ds \qquad (7)$$

Where V and S are the volume and surface of the magnet, J_m and j_m are their assumed current distribution, $B_{ext}$is the external magnetic field the magnet is subject to and r is the vector from the point about which the torque is computed.

The second methods instead reduces the magnet to a distribution of equivalent volume (ρ_m) and surface (σ_m) "magnetic charge" density that are used as the source term of the magnetostatic field equations. Their definitions are expressed

by equations 8 and 9 while the magnetic field can then be calculated with equation 10.

$$\rho_m = -\nabla \cdot M \quad (8)$$

$$\sigma_m = M \cdot \hat{n} \quad (9)$$

$$B(x) = \frac{\mu_0}{4\pi}\int_V \rho_m(x') \times \frac{(x-x')}{|x-x'|^3}\, dv + \frac{\mu_0}{4\pi}\oint_S \sigma_m(x') \times \frac{(x-x')}{|x-x'|^3}\, ds \quad (10)$$

As well, force and torque that a PM is subject due to the interaction with an external magnetic field B_{ext}, are obtained with equation 11 and 12.

$$F = \int_V \rho_m \times B_{ext}\, dv + \oint_S \sigma_m \times B_{ext}\, ds \qquad (11)$$

$$T = \int_V r \times (\rho_m \times B_{ext})\, dv + \oint_S r \times (\sigma_m \times B_{ext})\, ds \qquad (12)$$

The maximum torque that the actuation unit can generate on the IPM (T_{max}) at varying different distance can thus be obtained with different mathematical approaches that take in consideration the previous analysis of the problem.

Either Analytical Model or Finite Element Method (FEM) can be used.
In literature both the approached had been used for similar purposes: Furlani [35], analytically described the obtained generalized equation for a bipolar magnetic spur gear based on permanent magnets; Simi instead [36][37], used FEM methods for calculating attraction forces and triggering torque for a magnetic laparoscopic vision module and a magnetic spring capsule for non invasive biopsy.

The former method offers faster computational time but necessitate a mathematical formulation that requires advance mathematic since the problem cannot be solved in a straight forward manner but requires to split the problem

in two. It's in fact impossible to obtain the torque induced on a permanent magnet by another one: one must provide the free space magnetic field solution (B_{ext}) then the magnets where the torque is calculated must be reduced to equivalent current density or magnetic charges.
FEM method offers instead a simpler implementation focusing more on the geometry and parameters of the problem rather than the defining differential equation to describe it which are already included in most of the available software. Moreover, given the geometrical simplicity of the problem, the simulations can be performed with reasonable computational time.

Because of the pro's and con's of the possible approaches Comsol® 4.0 Multiphysics (Comsol inc. MA USA) had been chosen has software to implement FEM simulation.
Simulation that calculates the maximal induction torque between two ring shaped diametrically magnetized magnets, had been performed taking in consideration dimensions and magnetization value of commercially available Neodymium magnets.

Comsol provides simulation of different physical problems with a broad range of physical law already implemented and optimal visualization of the obtained results in terms of graphical output. To simply the simulation built and the parameters used, a schematic description of the steps used to implement the problem is provided with reference of the COMSOL Graphical User Interface (GUI), figure 2.3:

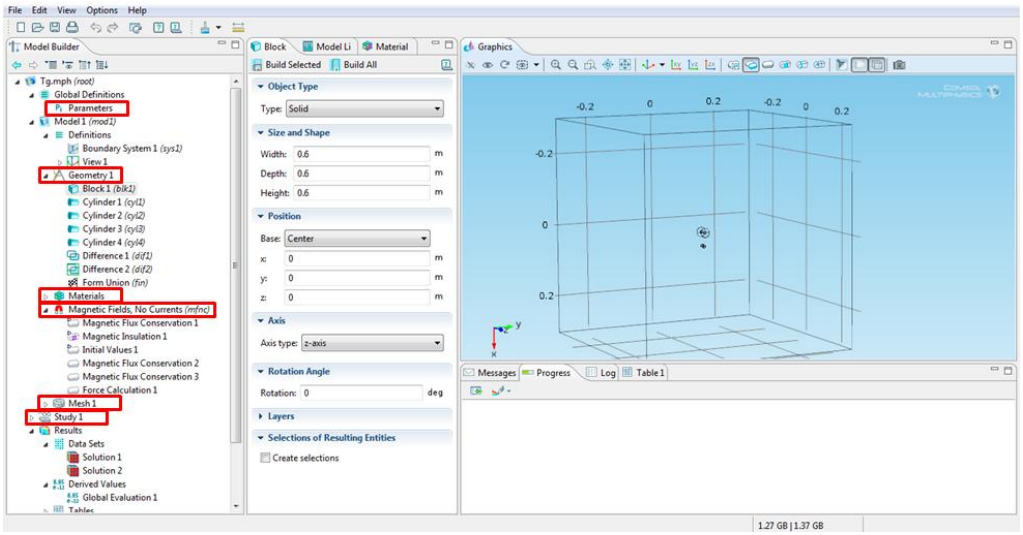

Figure 2.3: Comsol Gui with highlighted model builder's steps, that lead to the implementation of the simulation.

Definition of the physic of the problem

The correct physic of the problem must be selected. For the proposed simulation a

- 3D space dimension
- magnetic field no current (mfnc)
- stationary

problem has to be used.

Parameters definition

In order to easily determine the geometrical and magnetic properties of commercially available magnets, a parametric formulation guarantees a fast and precise method. Outside diameter, internal diameter, thickness, separation distance, magnetic field intensity of both EPM and IPM and their relative magnetic permeability had been included. The separation distance had been defined as the gap between the two facing surfaces of EPM and IPM.

Geometry of the problem

The simulation must be performed in an equivalent environment that simulate the free space where EPM and IPM are immersed in.

A 60 cm squared cube had been built with, in its middle, two ring shaped magnets laying on parallel axis with a starting separation distance between the facing surfaces of 2 cm. The cube dimension is at more than 10 times greater than the PM dimension.

To obtain a ring shaped geometry, that characterized both EPM and IPM, a boolean operation between two concentric cylindrical shape geometries had been necessary.

Material

The material property required to characterize the proposed physical problem is the relative magnetic permeability (μ/μ_0) of each components. The free space cubic geometry had been selected to be made of Air, material that had been selected from Cosmos material browser (relative magnetic permeability equals to 1). Both EPM and IPM had instead been characterized using a neodymium magnetic relative permeability value equals to 1.05.

Magnetic Field No Currents

The constitutive relations the two permanent magnets (equation 4) had been defined having magnetization in two perpendicular axis. With reference the 2D section of the model (figure 2.2), the EPM had been magnetized along y while the IPM along x.

The free space cube had instead been defined by default as magnetic insulator with null magnetic potential initial condition.

The calculation of the torque had been imposed using the IPM as reference magnet and its center of mass as the point about which the torque is computed.

Mesh

A user controlled mesh had been defined. EPM and IPM had been modeled with a mesh with a maximum element size of 0.05 mm and a minim element size of 0.005 mm with an element growth rate of 1.15. The cubic environment had instead been designed with 0.1 mm as a maximum element size and 0.01 mm as minimum element size with a growth factor of 1.25. The obtained mesh resulted composed by more than 3.500.000 elements.

Study

It's possible, with the use of the "Parametric sweep" option, to perform the same simulation with one parameter ranging from an initial value to a final one with a certain incremental step. A parametric sweep of the separation distance from the initial value of 2 cm to 10 cm with 0.2 cm as incremental step had been used to calculate the torque generated on the IPM at varying the separation distance.

Compute

The simulations run on a 16 Gb RAM computer and toke less than 10 minutes per separation distance thus a total time lower than 8 hours per simulation.

The obtained torque results for different couples of PM were exported and analyzed in Matlab®.

Dynamic Bench Test

In collaboration with my colleague Jacopo Buzzi, the selected PM had been dynamically characterized on a custom made bench test, figure 2.4.

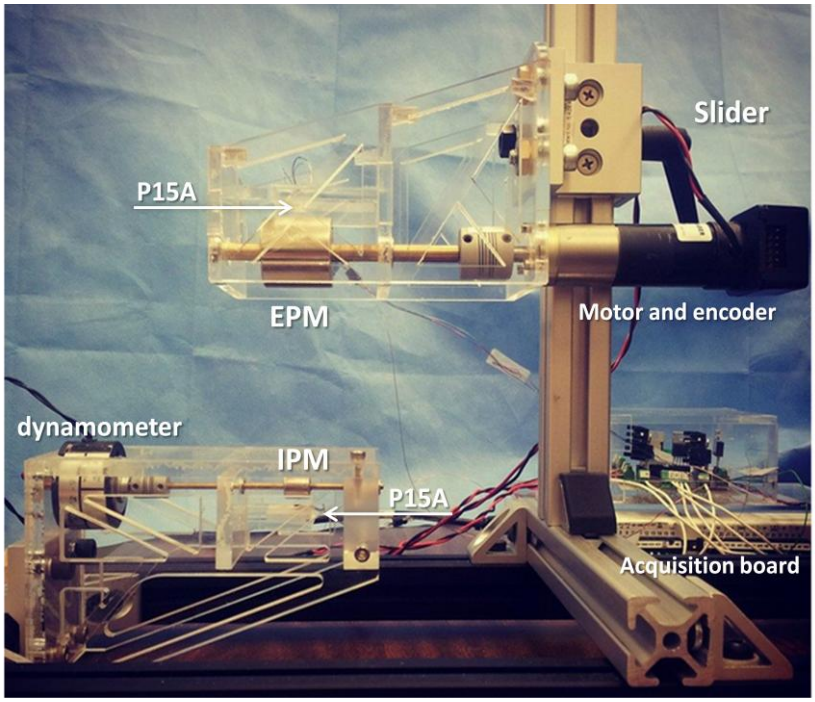

Figure 2.4: bench test utilized for dynamically characterize and study the selected actuation unit PMs. A motor mounted on a vertical slider is connected to the EPM. The IPM is connected to a dynamometer having the same EPM axis of rotation. Two hall effect sensors (P15A) are used to determine the angular position (θ_D and θ_d)of both the PM.

A faulhaber (2342S024CR 24V) electrical motor is rigidly connected to the EPM. They both are embedded on a Plexiglas case mounted on a vertical slider so that the EPM position (thus separation distance with respect of the IPM) can be changed manually with the use of a caliber.

The IPM is instead connected to a hysteresis brake dynamometer (Placid Industries H3 Hysteresis Brake) that impose a controllable load on it. As for the Motor-EPM, a Plexiglas's case had been built to contains all the components

and guarantee an alignment of the PMs rotation axis as assumed by the previous static model.

On the EPM side speed and torque had been acquired thanks to the motor optical encoder and the motor current monitor respectively. Dynamometer current output and magnetic field sensor (Hall Effect Sensor Element CY-P15A) have been used to obtain torque and speed on the IPM side.
All these information had been acquired with an hoc driver connected to a National Instruments DAQ (USB-6211). All the information about the driver, the acquisition strategy the utilized software to run the tests and the data analysis can be founded in Jacopo Buzzi MsC thesis.

Information of the possible transmittable torque at different separation distance and different speed regime are the main output the dynamic test is made for.
Five repetitions at different speeds (from 500 to 1700 rpm with 100 RPM step) and different separation distance (from 2 cm to 7 cm with 1cm step) had been tested while the load on the dynamometer was imposed to gradually increase until the - slippage condition – lose of power transmission [38] was achieved and recorded.

2.1.3 ACTUATION UNIT – RESULTS

Static Analysis

EPM and IPM had been selected and purchased (K&J Magnetics, Jaminson U.S).The selected EPM end IPM (figure 2.5) dimensions, magnetizations grade and price is listed in table 2.

	EPM	IPM
Outside Dia.	25.4 mm	9.525 mm
Inner Dia.	6.35 mm	2.38 mm
Thickness	25.4 mm	9.525 mm
Brmax	13 200 Gauss	13 200 Gauss
Magnetization grade	N42	N42
Price	22.77 $	1.67 $

Table 1: selected EPM and IPM of the actuation unit

Figure 2.5 purchased actuation unit couple of EPM and IPM (K&J Magnetics, Jaminson U.S).

The obtained torque (T_{max}) as simulation results for the chosen couple of permanent magnet is represented in figure 2.6.

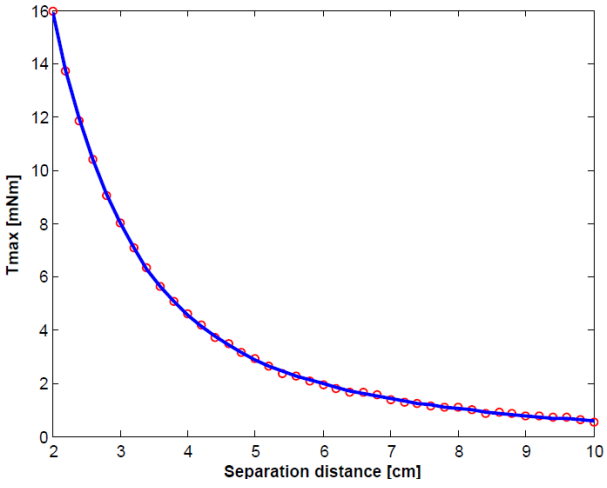

Figure 2.6: T_{max} at varying the separation distance. red dots: simulation data and in blue their exponential regression.

In Matlab the T_{max} at varying the separation distance (h) express in centimeters had been fit with a two member exponential regression, equation 3.

$$T_{max}(h) = -74.61 \cdot e^{-0.9702\,h} - 8.981 \cdot e^{-0.2726\,h} \qquad (13)$$

Dynamic Bench Test

Dynamically if the EPM is rotating in a clockwise direction, the IPM will follow in a counterclockwise fashion with the same angular velocity since the magnetic gear ratio is equal to 1.

As the load increases on the IPM side the dynamical behavior changes depending on the intensity of the applied load:

- If the torque imposed by the dynamometer is lower than the maximal transmissible torque (T_{max}) at the tested distance, the IPM is fully coupled with the EPM and the torque generation follows equation (1). The IPM overcomes the torque imposed by the load shifting its angular position in respect of the EPM one, thus increasing the angular displacement $\Delta\theta$ but maintaining the same angular velocity.
- If the load side exceed the torque transmission capacity of the actuation unit (T_{max}), the IPM enter a slipping condition [15], the coupling and thus the power transmission is lost.

Dynamically the maximal transmittable torque with respect of the simulations results has an efficiency of 86.66 ± 5.31% (Figure 2.7 a) while the variation of

the transmittable torque at increasing speed is not significant (figure 2.7 b).

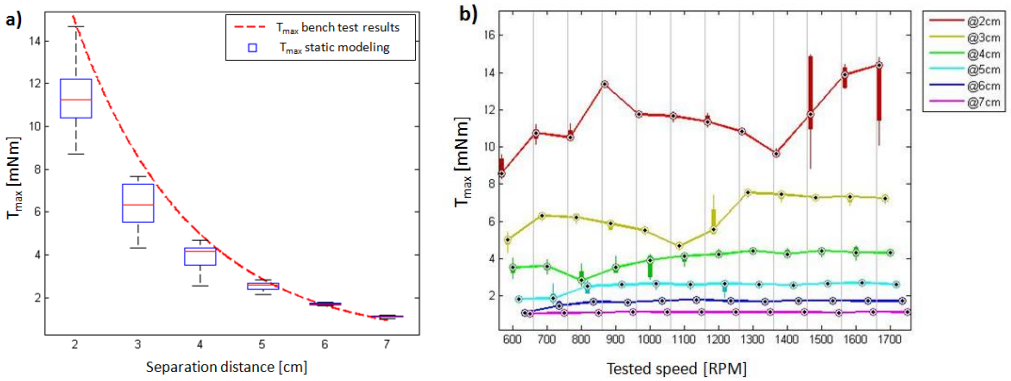

Figure 2.7: a) result of the dynamical study of torque transferring at varying the separation distance. In blue the bench test results, in red the static simulation regression line. b) result of the dynamical study of the torque transferring at varying the actuation unit velocity. Different color correspond constant separation distance.

2.1.4 ACTUATION UNIT - DISCUSSION

The selected magnets allow power transferring up to 7 cm as demonstrated by the dynamical test. The selected IPM can easily fit inside a 12 mm diameter device but the selected magnetization grade (N indicates its thermal characteristic) is guaranteed up to 80 degree. Nevertheless producer is able to treat neodymium magnets to achieve maximal operating temperature up to 200°C, making the selected magnets sterilizable with the high temperature techniques.

Dynamically the selected actuation unit had shown that the velocity do not interfere with the power transferring thus higher power can be obtained with higher velocity regimes. Commercially available micro motors with the same size of the IPM normally turns at a speed that is almost 10 times higher than the tested one. On the contrary their torque capacity are much lower than the one that the actuation unit is able to generate on the IPM. In particular, Maxon motors (www.maxonmotors.com), faulhaber motors (www.faulhabercom) and

Namiki precisions motors (Namiki.net), can continuously transmit at maximum 2.5 mNm, torque that is reached by the selected PM with 5.6 cm of separation distance.

The efficiency of the actuation unit as ratio between the dynamical transmitted torque and the static theoretical value decreases with the increase of the separation distance. At small separation distance the high magnetic forces induced strong vibration to the system letting the IPM enter in a slippage condition with in a broader torque range. Moreover the coupling condition allow not only torque transferring to the IPM but also on the EPM since is "magnetically" connected to the load side as verified by similar works [51]. At low distances the motor had been showed to slow down due to the increase of the load, and speed control strategy consequently implemented.
Montague et al. [39] had shown that a control strategy for magnetic coaxial spur gears is able to dynamically transmit up to 95% of the theoretical T_{max}.

2.2 PLANETARY GEARHEAD DESIGN

2.2.1 PLANETARY GEARHEAD INTRODUCTION

Technical requirement

Retractors requires high force at the instrument end effector and do not necessitate of a specific velocity to accomplish the retraction (CR5). The power that is transferred to the IPM must be converted into a slower and higher in torque one that can be transmitted to an actuation mechanism. Many are the possible solutions that can implemented, but few are the ones that can fit 12 mm diameter (CR2). A system that guarantee a high gear ratio (GR) with compact dimension, made of a material that does not interfere with the actuation unit, had be designed.

Description

The proposed solution is a planetary gearhead. They are widely used in micro robotic applications [40] because offer compact dimensions, large high-to-weight ratio, high efficiency and almost absent backslash. Because of the high gear ratio that can be reached in small dimension, investigation for fabricating mini-sized components are well established [41]. Commercially available planetary gear head are either in metallic material with high relative magnetic permeability and thus affected by the magnetic field or in plastics that have low mechanical properties. Because of these reasons a custom made planetary gear head that fit a 12 mm device had been designed, fabricated with a low relative magnetic permeability material and tested to mechanically characterize it.

A planetary gear is a particular configuration of epicyclical gears system and is composed by a sun gear (S), an annular gear (A), several planets (P), and a carrier (C) as represented in figure 2.8 a) and 2.8 b). Any of the carrier, annular

ring, and sun can be selected as the input or output component, and the power are transmitted through multiple paths of the planets meshes. The number of planets define the loadability of the system but a geometrical limit is given by gears dimension. The configuration in which the input gear is the sun, while the annular ring is fixed and thus the output gear of the system is the carrier (figure 2.8 c) permits to stack stages of planetary gears to form a planetary gearhead or planetary gearbox.

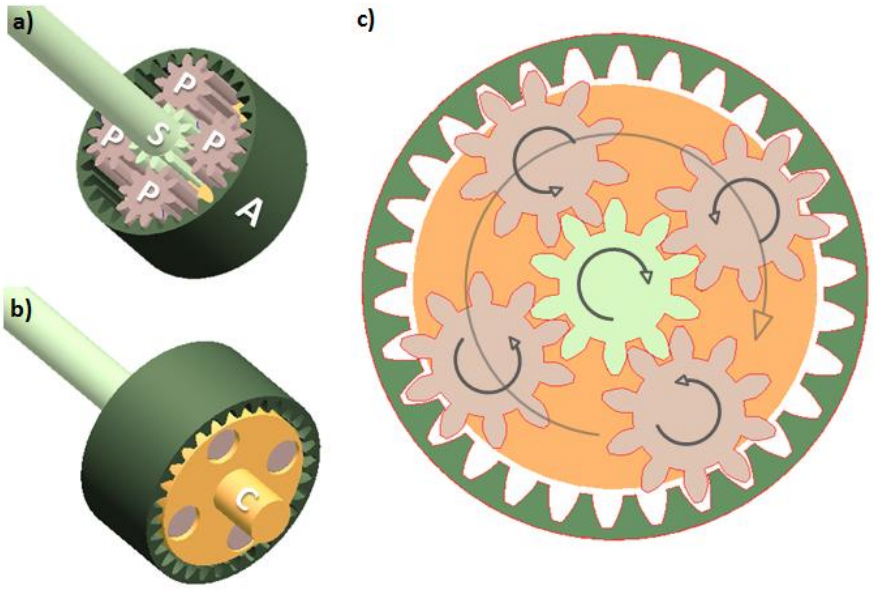

Figure 2.8: a) 3D rendering of an epicyclical gear with a planetary arrangement that show the position of sun (S), 4 planets (P) and annular gear (A). b) epicyclical gear where the carrier is highlighted to show how the planets mate with it. c) sense of rotation of each components of a planetary gear system when the annular gear motion is fixed.

Stacking multiple planetary gears to form a planetary gearhead offers the possibility to achieve very high gear ratio in compact size to detriment of the overall efficiency that is given by the product each stage efficiency.

To design a planetary gear, geometrical constrain are given for choosing the correct number of teeth that allow the system to work. Nevertheless teeth module and pressure angle are left free to the designer but have to be the same for all the components to guarantee perfect mating of each organ. The number of teeth of the annular ring ($Th_{annular}$) is determined by equation 14

$$\mathrm{Th}_{\,\mathrm{annular}} = \mathrm{Th}_{\mathrm{sun}} + 2 \cdot \mathrm{Th}_{\mathrm{planet}} \quad (14)$$

Where Th_{sun} is the number of teeth of the sun gear, Th_{planet} of the planets.

Moreover the configuration necessary to design a planetary gearhead where the annular ring is fixed (figure 2.8 c), has a GR per stage determined by equation 15.

$$GR_{\,singlestage} = 1 + \frac{Th_{annular}}{Th_{sun}} \quad (15)$$

2.2.2 PLANETARY GEAR HEAD - MATERIAL AND METHODS

A planetary gearhead had been designed in Pro Engineering Wildfire environment. To do so a parametric model of a spur gear had been implemented [42]. Spur gears have a very complex geometry determined by many variables. The most important parameters are:

- **Pitch circle**: An imaginary circle that contacts the pitch circle of any other gear with which it is in mesh.
- **Pitch diameter** (D): The diameter of the pitch circle.
- **Module** (m): The ratio of pitch diameter to the number of teeth. It is reciprocal of the diametral pitch.
- **Number of teeth** (Z): The number of teeth on the gear. equation 16

$$Z = D/m \quad (16)$$

- **Pressure angle** (Phi): The angle through which forces are transmitted between mating gears. Standard pressure angle is either 14.5°or 20°. It defines the tooth profile.

- **Tooth thickness** (B): thickness of the gear. With the teeth geometry and teeth number is the most important factor to define the gear loadability.

These parameter had been included in the Pro Engineering parametric tool. Others geometrical definition obtained from the defined parameters had been used to generate the involute profile of the teeth and, as visible from figure 2.9, cannot be modified in designed model. Gears geometrical definitions can be easily founded in any mechanical design hand book and are not here reported [43][44].

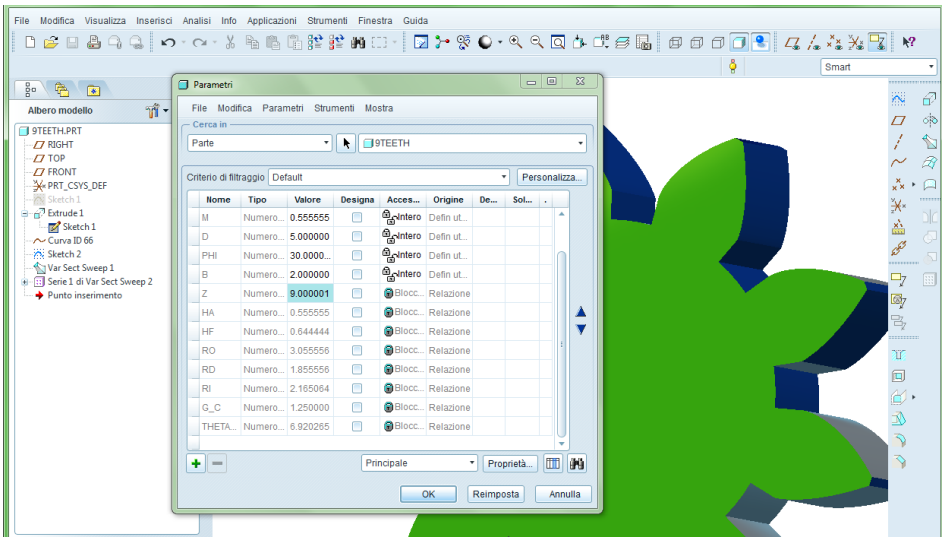

Figure 2.9: Pro/e snapshot of the parametric model of a spur gear.

With the proposed spur gear model the planetary gear head had been designed as assembly of different gears.

Gears are generally manufactured via hobbing that offers the possibility to obtain at minimum of 0.5 module teeth. Because of the dimension constrain a teeth module of 0.5 results excessive, thus a different solution for the fabrication had been investigated. The fabrication had been entrusted to “Technical machine

solution LLC" (Franklin TN) where wire cut Electrical Discharge Machining EDM method had been used. The EDM method is very precise and can ensure tolerances lower than 0.05 mm. Teeth profile requires a very high precision technique and gears efficiency deeply depends on it.

The fabricated gears loadability had been analytically estimated to define safe range of operation of the designed system. The Lewis's equation (equation 17) had been used to calculate the safe tooth load (W) and consequently estimate the maximal transmittable torque.

$$W = \frac{S \cdot B \cdot Y}{D_p} \qquad (17)$$

Where S is the maximum bending stress of the material [MPa], B the face width of gear [mm], Dp the diametral pitch [/] and Y the Lewis Form Factor [/].

The efficiency (η_{plan}) of the planetary gearhead cannot be calculated with analytical approach thus a specific bench test had been built to find it. Efficiency is calculated as ratio between output power ($\tau_{out}\omega_{out}$) and input power ($\tau_{in}\omega_{in}$) of the system (equation 18).

$$\eta_{plan} = \frac{P_{out}}{P_{in}} \cdot 100\ \% = \frac{\tau_{out}\omega_{out}}{\tau_{in}\omega_{in}} \cdot 100\ \% \qquad (18)$$

In a laser cut Plexiglas structure an electric motor (faulhaber 2342S024CR 24V) transfer the input power (speed and torque) to the planetary gearhead input component. The output one is instead connected to an hysteresis brake (placid industries B2) which is controlled to generate an increasing torque, figure 2.10.

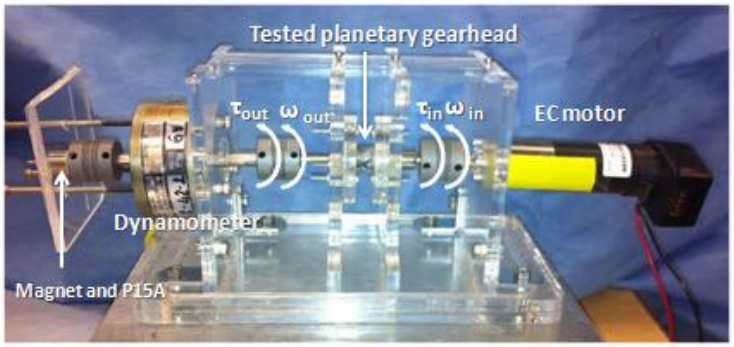

Figure 2.10: bench test used for calculating the efficiency of the designed planetary gearhead. An EC motor deliver input speed and input torque (τ_{in} and ω_{in}) to the planetary gearhead system, the dynamometer represent the output load τ_{out}. Connected to the dynamometer shaft a PM is used to measure the output velocity ω_{out}.

The motor information referred as τ_{in} and ω_{in}, had been acquired from current monitor and the motor optical encoder respectively. The same information on the load side had been obtained from the current monitor of the dynamometer and from a hall effect magnetic field sensor (P15A) that measured the magnetic field of a diametrically magnetized magnets which rotates concordant with the dynamometer shaft.

Five repetitions where the motor had been set to 1700 RPM and the load imposed to raise from 8.17 mNm to 80 mNm in 10 seconds had been recorded and the data post processed in Matlab.

2.2.3 PLANETARY GEARHEAD – RESULTS

The designed planetary gear head is composed by three identical stages, each of them contains a 3.2mm D sun gear, four planets with 3.2 mm D and an annular ring of 9.85 mm D. The teeth had been selected to have a module of 0.32 with a pressure angle of 22.5° and are 10 on the sun and planet gears and 30 on the

annular ring. Each stage has thus a individual GR of 4:1, while the planetary gearhead total GR is 64:1.

The gears thickness had been chosen to be 3.125 mm in order to increase the mating surface, decrease the local stress on the teeth and thus increase the loadability of the system. For the same reasons the number of planets of each stage had been set to 4.

In order to assemble the three stages, the carrier output of the each stage had been mated with the input sun of the next stage, figure 2.11.

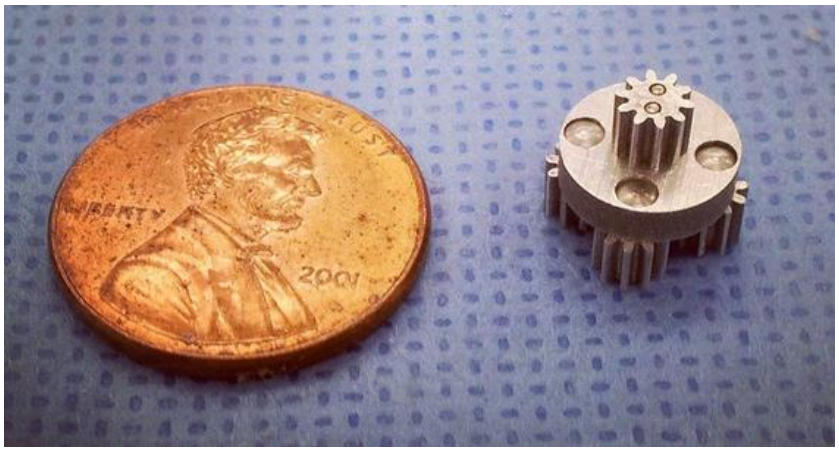

Figure 2.11: designed carrier assembled with the sun on top thanks to two 0.8 mm stainless steel pins and the four planets that mate thought 2 mm holes.

The planets mate with the carrier through a pin of 2 mm diameter and the carrier thickness had been chosen to be 2.38 mm.

One annular ring with an outside diameter of 11 mm and a thickness of 17 mm accommodates all the three stages.

The fabrication material had been Aluminum Al 6061-T6:

- Tensile strength - yield 276 MPa;
- Tensile strength - ultimate 310MPa;
- Relative magnetic permeability 1.004.

This specific type of aluminum is commonly used in Aerospatiale applications since offers low weight and increased mechanical properties. A relative magnetic permeability of 1.004 guarantees absent magnetic susceptibility and no interference with the magnetic field of the actuation unit IPM the planetary gearhead is connected to. In figure 2.12 the fabricated part before the assembly are showed.

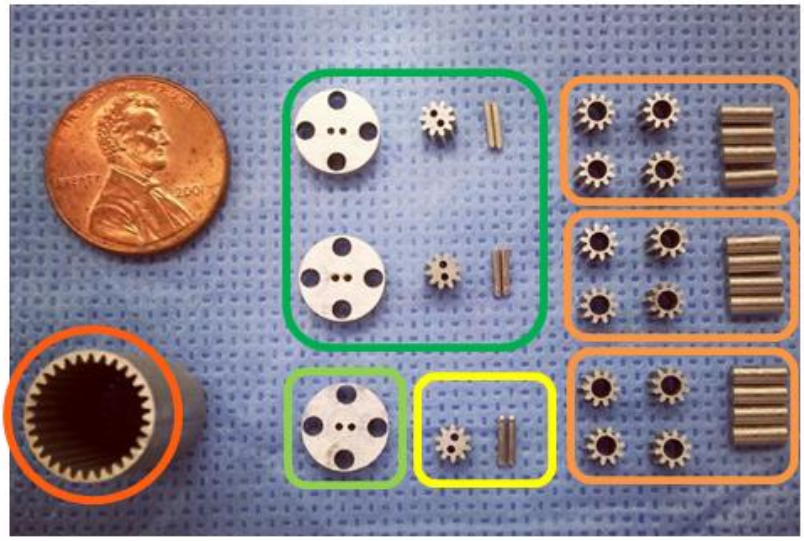

Figure 2.12 : components of the designed planetary gearhead before assembly. Yellow: input sun; dark green: carriers with the next stage sun; light green: last carrier thus output of the system; orange: planets, red: annular ring.

The part had been assembled with purchased (McMaster, Elmhurst, U.S.) austenitic stainless steel (relative magnetic permeability 2.05) pins (0.8 mm φ x 5 mm long and 2 mm φ x 5 mm long).

Two 0.8 diameter holes at 1.25 mm of distance had been obtained in each sun and carrier center and the 0.8 mm diameter pins used to mate:

- The first sun with the IPM shaft;
- the second and the third sun with the previous stage carrier (figure 2.11);
- the last carrier with the next mechanical train component.

Stainless steel has much higher mechanical properties than aluminum but is harder to machine, torque is transferred without breakage since the weakest point had been assumed to be the gear teeth.
The 2 mm diameter and 5 mm long pins had instead been used to fit the planets holes and thus assemble the planet gears. A medical purpose glue, Loctite 4041, had been used to mates all the components.

From the material mechanical properties a safe tooth load of 21.09N had been calculated. Since pitch radius is 1.6 mm the safe tooth transmittable torque is 33.74 mNm. Choosing a four planets arrangement for each stage guarantee a higher loadability, the maximum safe torque of the system results 134.96 mNm.

The assembled planetary gearhead had been greased with a general purpose lubricant (MG Chemicals white lithium grease) and the bench test run.

The measured efficiency of the system had been: 61.25 ± 3.16%.

2.2.4 PLANETARY GEARHEAD - DISCUSSION

A 11 mm diameter and 17 mm long planetary gearhead with a 64:1 GR and an efficiency of 61.25% had been designed and fabricated in Al-6061-T6. The proposed design, thanks to wide teeth and a 4 planets arrangement is able to transmit theoretically a safe torque of 134.96mNm. Commercially available planetary gearhead (falhauber planetary gear head series 10/1) with similar dimensions guarantee a safe maximal continuous torque up to 100 mNm and an intermittent torque of 150 mNm with an efficiency of 70%.
Further analysis to quantify performance of the designed system must be performed for more qualitative results. Since the CAD files of the designed

planetary gearhead are available, a Finite Element Methods can be used to verify the calculated safe torque.

2.3 POWER SCREW

2.3.1 POWER SCREW INTRODUCTION

Technical requirement

The converted power coming from the planetary gearhead described in the previous section is transmitted to an actuation system that must guarantee the retraction of a mass that weight up to 750 grams (CR5). From the possible solutions only those that can fit a 12 mm diameter device (CR2) are selectable. The mechanical material must be inert to magnetic fields.

Description

To better exploit the dimensions a power screw integrated with an offset crank mechanism (section 2.4) is the solution proposed. Power screw (PS) are generally used to obtain high mechanical advantage for moving large loads with minimum effort, generate large force and obtain precise axial movement with compact dimension.

PS or lead screw converts rotational motion of a screw component in linear motion of the mating nut. It can be backdrivable or non-backdrivable depending on its design parameters [45]. To secure the retracted tissue once the retraction had been performed a self locking (i.e. non back drivable) solution is preferred. The transmitted power is used only for retracting, while holding can be mechanically ensured by the screw-nut mating.

Commercially available PS can fit inside a 12 mm device but requires machine procedure to connect with the designed planetary gearhead and even more complex procedure to integrate with an offset crank mechanism. Hence a PS that integrates with the previous component of the mechanical train and can integrate with an offset crank mechanism had been designed, fabricated and tested.

Power screw is mechanically characterized by its geometrical parameters (figure 2.13):

- **Dm**: Pitch diameter. Screw equivalent diameter that can be taken in consideration to study where the forces are transmitted.
- **P**: pitch. the distance along the screw's axis that is covered by one complete rotation of the screw.
- **α**: Lead angle, can be geometrically calculated from the Dm and the P. It effects the mechanical advantage and the efficiency of the PS.
- **θ**: thread angle. Is the angle that determine how the forces between screw and nut are transmitted. Different thread solutions can be designed such as metric, squared, ACME buttress. In the proposed design standard ACME profile have been analyzed cause are the easiest one to machine.

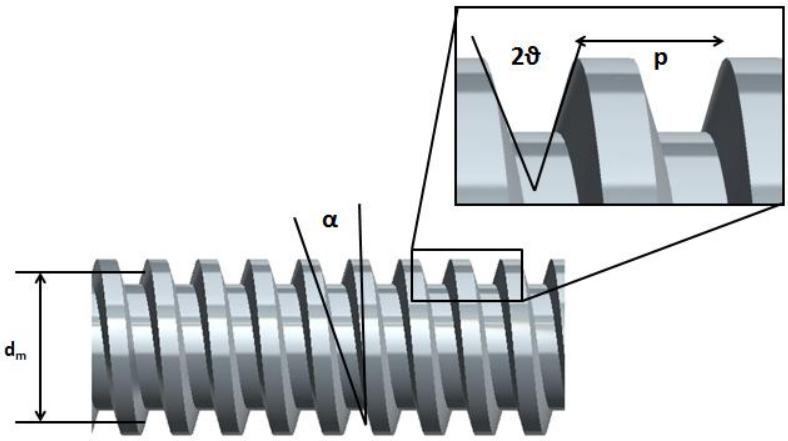

Figure 2.13: PS parameters and their geometrical meaning from a Pro Engineering snapshot.

2.3.2 POWER SCREW – MATERIAL AND METHOD

In Pro Engineering Wildfire environment a non back drivable power screw that integrates with the planetary gearhead. Consequently, a mating nut properly designed to actuate a slider crank mechanism inside a 12 mm device had been

obtained. Its fabrication had been entrusted to the Vanderbilt University machine shop (Stevenson center – room 6316).

Power screw performances depend on the designed geometrical parameter and on the lubrication regime. Analytical equations (equation 19 and 20) had been used to calculate the required torque (T_r) for raising a load (retract the tissue) and to estimate the system efficiency (η_{ps}) [24].

$$T_r = \frac{d_m \cdot W}{2}\left[\frac{\mu_s + \cos\theta \cdot \tan\alpha}{\cos\theta - \mu_s \cdot \tan\alpha}\right] + \frac{d_{mc}\,\mu_c W}{2} \qquad (19)$$

$$\eta_{ps} = \frac{\cos\theta - \mu_s \cdot \tan\alpha}{\cos\theta + \mu_s \cdot \cot\alpha} \qquad (20)$$

where W represent the weight to lift, $d_{mc}$the mean collar diameter, μ_s represent the static friction coefficient between screw and nut, μ_c the static friction coefficient at the collar surface.

From equation 19 a transfer function β_{lead}, that convert input torque [mNm] into raising force [N] had been defined (equation 21):

$$\beta_{lead} = \frac{\text{OUTPUT force}}{\text{INPUT torque}} = \left[{}^{N}/_{mNm}\right] \quad (21)$$

The efficiency of the fabricated power screw had also been verified with a weight lifting tests. In a Plexiglas laser cut assembled case, a faulhaber 2342S024CR motor rigidly connects to the power screw placed in a vertical position. A known weight (F_{load}) ranging from 0.4535 kg to 4.5349 kg with 0.4535 kg incremental step, had been applied on the nut and the torque (τ_{mot}) request by the motor had been recorded from the motor current monitor with the same hardware and software utilized in the actuation unit dynamical tests. Figure 2.14.

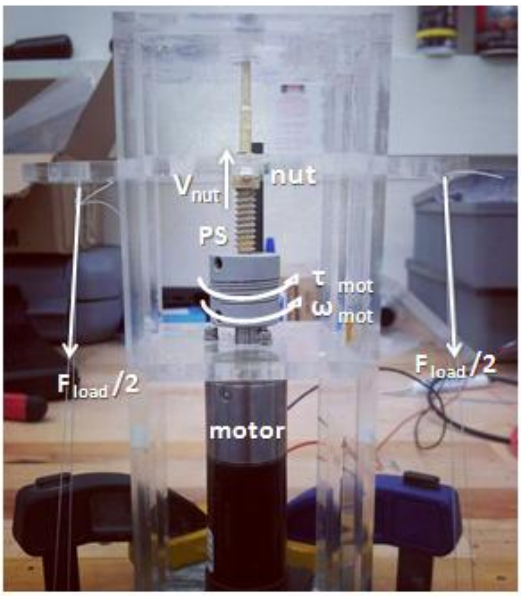

Figure 2.14: bench test utilized to measure the designed lead screw efficiency. A EC motor transfer input speed ω_{mot} and torque τ_{mot} to the PS. The PS is requested to lift a known weight F_{load} .

The efficiency (η_{pstest}) had been calculated with the assumption that the system is infinitely rigid and thus with no lose in speed.

The velocity of the PS nut (V_{nut}) had been simplified with the angular velocity of the motor (ω_{mot}) knowing the pitch (P) of the PS, see equation 22.

$$V_{nut}\left[\frac{mm}{sec}\right] = \omega_{mot}\left[\frac{round}{sec}\right] \cdot pitch\left[\frac{mm}{round}\right] \qquad (22)$$

The measured efficiency is expressed in equation 23:

$$\eta_{pstest} = \frac{F_{nut}V_{nut}}{\tau_{mot}\omega_{mot}} \cdot 100\ \% = \frac{F_{load} \cdot P}{\tau_{mot}} \cdot 100\ \% \qquad (23)$$

Three repetition per weight had been performed and the acquired data analyzed in Matlab.

2.3.3 POWER SCREW – RESULTS

A single thread, 4.8 mm pitch diameter (dm) with a 1.5875 pitch (P), 30° ACME thread angle (ϑ) with resultant lead angle (α) of 18.3° had been designed. The

length of the lead had been chosen to be 25 mm the explanation of this parameter will be discussed in section 2.4.3. Two shafts 3 mm diameter and 5 mm long had been added at the screw extremity to mate with the planetary gearhead on one side and to mate with the device body on the other side. A 7mm squared nuts, 6 mm thick with the same thread been designed as the mating nut, figure 2.15 a). Two sides of the squared nut had been used prevent nut rotation, the other two side had instead designed with two 2 mm diameter pins that are used to integrate with the offset crank mechanism see figure 2.15 b).

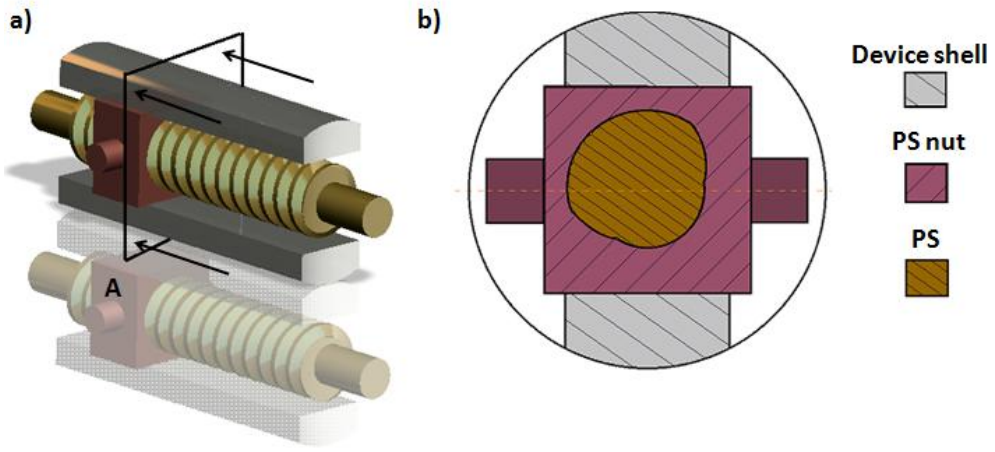

Figure 2.15: a) Pro Engineering rendering of the designed PS and nut inside the device. b) section A of the assembly to show the components arrangement inside the device body.

The proposed solution can easily fit inside a 12 mm diameter device as showed in result visible. The reasons that had led to chose the visibility of the components are stated in section 2.4.4.

The parts were fabricated in brass because of its easiness to be machined, the non magnetic and mechanical properties of the material:

- Tensile strength - yield 310 MPa;
- Tensile strength - ultimate 476MPa;
- Relative magnetic permeability 1.06.

The shaft extremity that mates the planetary gearhead output, two holes of 0.8 mm diameter at 1.25 mm of distance had been drilled for connecting the pins as described in the assembly of the planetary gearhead (section 2.2.3).

For the analytical calculation the value of static friction $\mu_s$had been estimated. Chowdhury et al. [46] had investigated the brass to brass friction coefficient and reported a value of 0.1. Since the parts had been tested with the use a general purpose lubricant (MG Chemicals white lithium grease) a value of μ_s equals to 0.095 had been used.

To calculated maximum force that the nut is able to exert a simplification had been included: the collar interaction (equation 19) had been considered neglectable since the PS is embedded in Delrin bearings (see section 2.6) at the shafts extremities that offer optimal lubrication and wear resistance.

The resultant force, given the maximum torque that can be transmitted by the planetary gearhead (134.96 mNm), is 123.01N. The resultant nut velocity given the maximum actuation unit speed (1700 RPM) results 0.708 mm/sec.

The analytical efficiency results 72.73% while the transfer function β_{lead} is equal to 0.9117 $[N/mNm]$.

The efficiency obtained with the proposed lifting test results 69.85 ± 5.44%, in agreement with the analytical calculation.

2.3.4 POWER SCREW – DISCUSSION

A 4.8 mm pitch diameter non back drivable power screw with an efficiency of 69.85% had been designed and fabricated. The compact dimension and high mechanical advantage obtained from the design parameter permits to generate, given the input speed and torque coming from the planetary gearhead a maximal output force of 123.01 at 0.708 mm/s.

No analytical calculation neither FEM simulation had been used to calculate the mechanical stresses on the teeth since the planetary gearhead had been assumed to be the weakest component of the mechanical train thus the first to eventually run into failure.

Future studies expect to optimize the design starting from mechanical stresses analysis so that the geometrical dimensions and teeth form can be to optimized or even decrease.

2.4 OFFSET CRANK MECHANISM

2.4.1 OFFSET CRANK- INTRODUCTION

Technical requirement

The PS had been demonstrated to generate high output force and slow nut motion. The offset crank mechanism introduced previously, has thus to integrate with the PS and generate high forces at a retracting lever tip. The lever must be properly designed to integrated with the mechanism components and retract masses up to 750 grams (CR5) with a reasonable displacement but compact dimensions (CR6). All the parts that compose an offset crank mechanism, have to fit the dimension constrains (CR 2) and be made of a material with a low magnetic susceptibility to do not interfere with the magnetic fields generated by the magnetic unit.

Description

The proposed mechanical solution is an offset crank mechanism that integrates with the PS nut, that act as slider, while the crank component is united with the retracting lever.

Crank slider mechanism are used to convert a sliding motion of the slider into a rotational one (crank) through connecting rods. The term offset refers to the crank mechanism when the slider line of action has an offset with respect of the hinged extremity of the crank. The slider line of action is in the center of the device section while the crank components has to be hinged in one of the device extremity to better exploit the available space.

2.4.2 OFFSET CRANK – MATERIAL AND METHODS

To determine the optimal initial configuration and lengths of the offset crank components a two step kinematic study in Matlab had been performed.

1 A **displacement analysis,** to obtain the link positions during the simulation motion of a generic offset crank mechanism, had been performed with the use of the vector loop equations [47][48], figure 2.16.

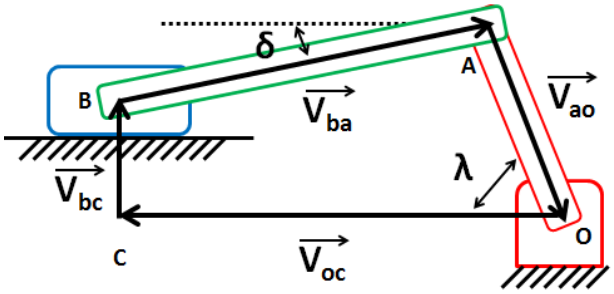

Figure 2.16: schematic representation of the vector loop approached used to solve the offset crank mechanism displacement analysis. In blue the slider, in green the connecting rod, in red the crank.

In the proposed case the input parameter of the system had been the position of the slider (V_{oc}), from it, the unknown angular displacement δ and λ had been be obtained. The length of the components (V_{ba} ; V_{ao}) and the offset (V_{bc}) are assumed constant thus the position of each joint during the motion can be derived.

In particular the angular position δ and λ during the slider motion V_{oc} can be calculated with equation 24 and equation 25.

$$\delta = \frac{2\tan^{-1}\left(-2V_{ao}V_{bc} - \sqrt{(-2V_{oc}V_{ao})^2 + (2V_{ao}V_{bc})^2 - \left(V_{oc}^2 + V_{bc}^2 + V_{ao}^2 - V_{ba}^2\right)^2}\right)}{-2V_{oc}V_{ao} - V_{oc}^2 - V_{bc}^2 - V_{ao}^2 + V_{ba}^2} \quad (24)$$

$$\lambda = \frac{2\tan^{-1}\left(-2V_{ba}V_{bc} - \sqrt{(-2V_{oc}V_{ba})^2 + (2V_{ab}V_{bc})^2 - \left(V_{oc}^2 + V_{bc}^2 + V_{ba}^2 - V_{ao}^2\right)^2}\right)}{-2V_{oc}V_{ba} - V_{oc}^2 - V_{bc}^2 - V_{ba}^2 + V_{ao}^2} \quad (25)$$

Since the retraction is performed by a retracting lever united to the crank component and the obtained displacement depends on its length and angular displacement, the required output of the system had been an angular λ

displacement of 90°. The retracting lever is thus able to open and after clutching the tissue with and optimal wire length, perform the retraction due to its closure.

2 A **force analysis** had instead been used to calculate the torque generated on the crank (T) due to the input force (F) acting on the slider [47] [48]. Because of the slow velocity of the joints (nut motion 0.708 mm/sec) a static analysis had been performed assuming neglectable the inertia components of the links. For each link the static cardinal equations had been derived from the free body diagram (figure 2.17). These 9 equation had been put in a matrix form in Matlab where the unknown kept on the left hand side while the known input force (F) placed on the right hand side.

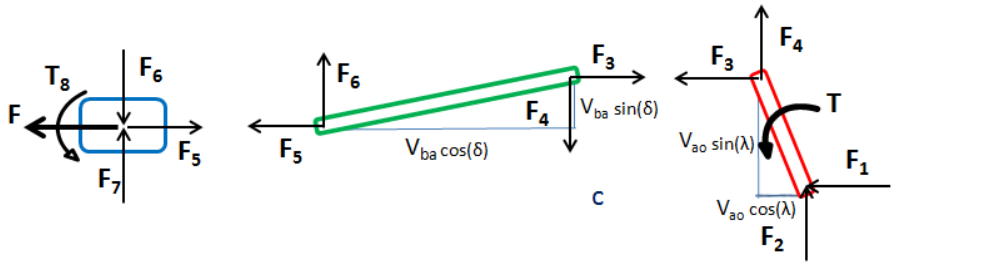

$-F_5 + F = 0$
$-F_6 + F_7 = 0$
$T_8 = 0$

$-F_3 + F_5 = 0$
$-F_4 + F_6 = 0$
$V_{ba}\ sin(\delta)F_5 + V_{ba}cos(\delta)F_6 + T = 0$

$F_1 + F_3 = 0$
$F_2 + F_2 = 0$
$-V_{ao}\ sin(\lambda)F_3 + Vaocos(\lambda)F_4 + T = 0$

Figure 2.17: free body diagram and static cardinal equation of each offset crank link used for the force analysis.

The output torque (T) had been obtained substituting the link displacement previously calculated ($V_{oc,}$ δ and λ) during the simulated motion. Using a unitary applied force (F) a transfer function Γ, calculated as ratio between the output torque on the crank (T) and the input force (F), had been deduced (equation 26).

$$\Gamma = \frac{\mathrm{T(output\ torque)}}{\mathrm{F\ (input\ force)}} = \left[{}^{\mathrm{mNm}}/_{\mathrm{N}}\right] \quad (26)$$

The link had been designed in Pro Engineering Wildfire with the optimal length calculated from the kinematic analysis. The designed parts have to integrate with the PS nut-slider, include a retracting lever at the crank component and fit inside the 12 mm device.

The designed parts were fabricated by the Vanderbilt University machine shop (Stevenson center – room 6316).

2.4.3 OFFSET CRANK – RESULTS

The links lengths had been selected taking in consideration that the connecting rod has to be long enough to do avoid interference with the PS length, the crank component has to be smaller than 12 mm. The chosen length and initial angle configuration are showed in figure 2.18 a) while a Matlab simulated motion is represented in figure 2.18 b).

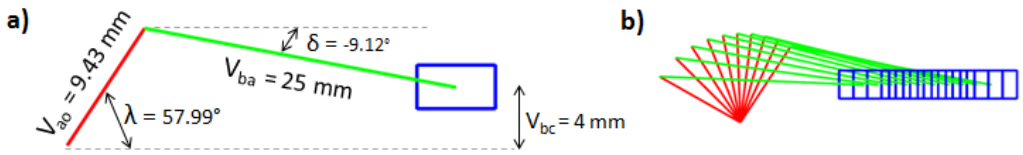

Figure 2.18: a) initial configuration of the link studied in Matlab, b) Matlab motion simulation.

To generate an angular displacement of λ of 90°, the slider ($V_{oc)}$ has to move 12.71 mm from the initial configuration. The PS length of 25mm ensure the requested linear displacement of the nut-slider with enough tolerance. Given the nut speed, the mechanism requires 18.07 sec to accomplish the selected range of motion and the crank velocity that can be assumed constant in the studied range is 0.83RPM.

The proposed initial configuration guarantee that the crank has an initial height of 8 mm and thus satisfy the geometrical constrain.

The joints range of motion and the transfer function Γ during the simulated motion are showed in figure 2.19.

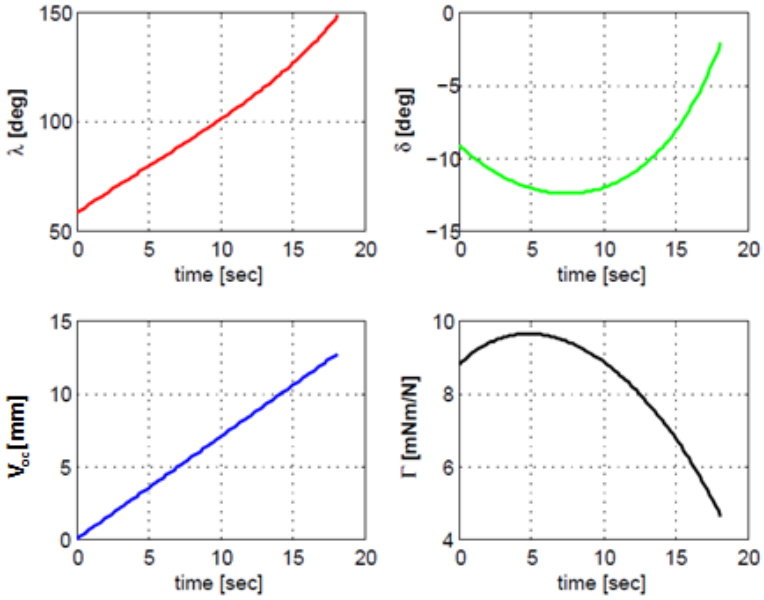

Figure 2.19: offset crank mechanism joint motion and mechanical advantage function. top left: the angular displacement over time of the crank angle λ; top right: the angular displacement over time of the connecting rod angle δ; bottom left: slider displacement (V_{oc}); bottom right: transfer function Γ during the studied mechanism dynamic.

The retracting lever is united with the crank components thus its relative angular displacement (γ) can be defined with respect of the crank one (λ). It results 0 degree at the initial configuration (closed lever) and 90 degree at the end of the simulated cycle (open lever), equation 27.

$$\gamma(t) = \lambda(t) - \lambda_{ini} \quad (27)$$

The transfer function Γ is no constant over the studied cycle, it reaches a maximum point of 9.63 mNm/N when the lever angular displacement γ is 21.17° and has a minimum point (4.67mNm/N) when γ is 90° thus at the end of the studied cycle and at fully open configuration of the lever.

In Matlab the function Γ at varying the angle γ had been obtained as polynomial regression of the third grade (R^2=0.99), equation 28.

$$\Gamma(\gamma) = 1.985\,\gamma^3 - 7.917\,\gamma^2 + 4.935\,\gamma + 8.797 \quad (28)$$

Velocity and acceleration had also been calculated from the obtained kinematic but are not here reported either discussed since are neglectable (velocities lower than 0.15 rad/sec, accelerations lower than 0.005 rad/sec^2) and thus confirm the static approach assumption used in the force analysis.

The offset crank links had been designed taking particular attention to their space arrangement. A retracting lever of 58.5 mm had been included in the design of the crank, figure 2.20.

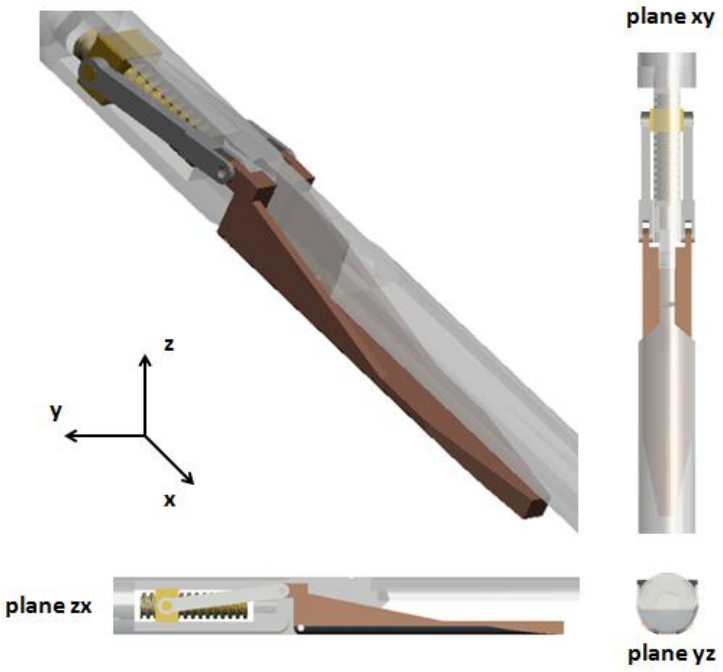

Figure 2.20: 3D rendering and 2D projections of the offset crank links. The connecting rod (grey) mate with the slider nut, while the crank (brown) include a 58.5 mm retracting lever.

Two connecting rods that couple with the PS-nut pins balance the nut motion and split the transmitted forces in two, diminishing the stresses acting on them and on the connecting pins.
The retracting lever, that undergoes a 90° angular displacement from a closed position to an open one, had been designed to mate with the two connecting rods and rotate about a hinge point at the device body. Buttresses had been included to guarantee bending resistance of the lever.
The offset crank mechanism is visible since the components motion would have been limited by a thin device outer layer. Moreover, the device body structural resistance is guarantee by a thick extrusion in the core of the device while the components are arranged around it.

From the kinematic calculation and the maximal input force that can be transmitted by the PS, is possible to predict the maximal torque T of the crank and thus at the lever tip. The retracting solution allow to consider the retracted mass as concentrated on the lever tip.
With a maximal input force (F) of 85.44 N (123.01 N * η_{pstest}) coming from the PS-nut, a retracting lever length of 58.5 mm and mechanical transfer function Γ (equation 28), is possible to predict the obtained force at the lever tip during the retraction. At γ = 90 a force of 6.82 N is theoretically generated, while at γ = 21.17° (Γ maximum) the force results 14.06 N.

The parts fabricated in aluminum 6061-T1, that has high workability and low magnetic susceptibility, are showed in assembled configuration in figure 2.21.

Figure 2.21: assembled configuration of the fabricated offset crank links mating with the PS nut.

To assemble the mechanism stainless steel 316 pins of 1.5 mm diameter had been used to connect the connecting rods to the crank-retracting lever while a 1 mm diameter pin represents the hinge point of the crank.

2.4.4 OFFSET CRANK DISCUSSION

An offset crank mechanism that permits an angular displacement of 90 degree of a retracting lever of 58.5 mm integrated in the crank component had been designed and fabricated. The components arrangement had been studied to better exploit the limited space.

The torque generated by the crank, converted into a force acting at the lever's tip, increase while the lever closes – retraction is performed. The maximum weight that can be retracted passes from a minimum value of 695 g at fully open configuration (γ = 90 degree) to a maximum of 1443 gr (γ = 21.17 degree). Because of the retracting approach, the retracted tissues undergo to vertical displacement of 58.5 mm in 18.07 sec.

Stresses analysis had not been performed because the weakest component has been considered to the planetary gearhead teeth. Future development includes the optimization of the components dimension with analytical stress calculation. The links can be easily described with analytical stress calculation, avoiding time consuming FEM simulation.

2.5 ANCHORING UNIT

2.5.1 ANCHORING UNIT - INTRODUCTION

Tech requirements

New generation of PM are able to generate high attraction forces across physical barriers. The anchoring unit must be dimensioned to unload the retracted tissue (CR5) and allow workspace exploration (CR6) for optimal positioning of the internal device, within a clinical relevant range of abdominal thickness (CR1).
The magnetic attraction has to be present up to 4 cm but the generated pressure on the abdominal wall never results harmful for the patient (CR4).
As for the actuation unit, the IPM has to be smaller than 12 mm in diameter while the EPM does not have dimensional limitation and both have to resist high temperature sterilization.

Description

The attraction force at varying the separation distance acting on the IPM has to be calculated. Block permanent magnets had been showed able to generate higher attraction forces than cylindrical shape one with the same volume [49]. Hence the analysis has been performed among commercially available block neodymium magnets.

Despite the unloading function, the anchoring unit also has to ensure a stable motion for workspace exploration. A magnetic levitation system that ensure motion of magnetically anchored device inside the abdominal wall without losing attraction had been studied and analyzed in the magnetic camera robot by Simi [36], the verification had been performed following the same approach.
The magnetic dragging force (F_{drag}) generated by a misalignment (m) between EPM and IPM relative position of their center of mass, at a fixed separation

distance (d) has to overcome the friction force (F_f) calculated as the product between the attraction force (F_a) and the static friction coefficient of the abdominal wall (μ_{abd}), figure 2.22.

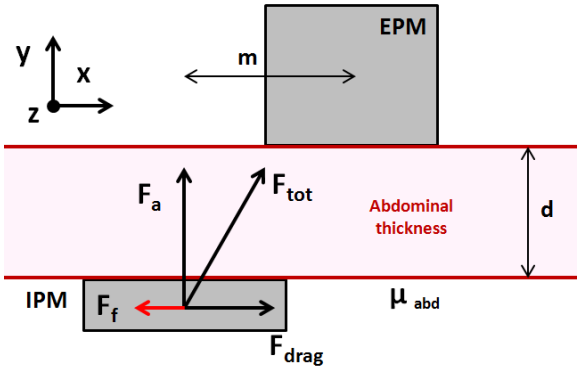

Figure 2.22: 2D representation of the magnetic levitation system analysis to verify magnetically anchored devices motion.

To verify the motion, information about the attraction force (F_a) and the dragging force (F_{drag}) at varying the misalignment distance (m) must be calculated.

The Anchoring unit IPM position inside the device has to be studied as well. Two IPMs (the Actuation unit and the Anchoring one) are in fact embedded in the insertable device and they both are subject to attraction forces (F_{Act} and F_{Anc} respectively) thus an equivalent structural model that can predict the retraction capacity of the device can be defined.

The actuation unit is able not only to transfer wirelessly torque on the IPM but also to generate attraction on it. The intensity of the generate force is much lower than the anchoring unit one but it cannot be neglected and thus must be considered for studying the device holding capability.

The device can be modeled as a beam with two attraction forces (F_{Act} and F_{Anc}) direct upward located at the IPMs center of mass while the retracted tissue weight force (F_W) located at the retracting lever tip can be ideally assumed as directed downward (figure 2.23 a).

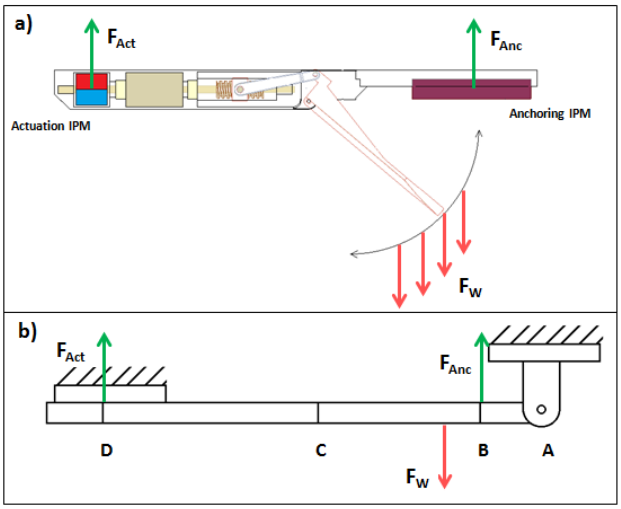

Figure 2.23: a) schematic representation of the device where the force are modeled. b) equivalent structural model of the device used to evaluate the device performance, D: center of mass of the actuation unit IPM, C hinge point of the retracting lever, B center of mass of the anchoring unit IPM, A device edge.

The device results attracted to the abdominal wall by two off-centered vertical forces thus the degree of freedom, that a vertical F_W force can actuate, is the rotation in respect with one of the device extremity. No forces along x direction have been considered.

If the Actuation unit attraction force is assumed constant and lower than the anchoring unit one and the F_W force is placed in between those two forces, the static cardinal equations tell that motion occurs on the Anchoring unit extremity (A) that acts as hinge point, Figure 2.23 b.

The more instable case is when the F_W force acts on the retracting lever hinge point (C) since its momentum is maximum.

Static equilibrium is thus ensured if the F_W momentum is lower than the equivalent attraction one, equation 29:

$$F_w < \frac{F_{Anc} \cdot AB + F_{Act} \cdot AD}{AC} \qquad (29)$$

where AB is the distance in mm between the device edge and the anchoring IPM center of mass, AD is the distance between the device edge and the actuation unit IPM center of mass, AC is the distance between the device edge and hinge point of the retracting lever.

In the following section the:

- attraction force acting on the anchoring unit IPM is calculated at varying the separation distance between commercially available PM to select the EPM and IPM;
- the IPM motion inside the abdominal cavity, with the Simi [36] approach, is verified;
- the structural model here presented is tested and validate.

2.5.2 ANCHORING UNIT- MATERIAL AND METHODS

Attraction Forces

The magnetostatic problem of calculating the attraction force that a PM is able to exert on another PM at different separation distance starts from the Maxwell's equation analysis explained for the actuation unit torque calculation (section 2.1.1) equations (6) and (11).

Again FEM simulation in Comsol Multiphysics is the selected program. The anchoring unit had been dimensioned with series of 3D simulation among commercially available Neodymium block PM.

The same steps utilized to define the simulation described in section 2.1.2, had been used. Differently the magnetization of two block PM had been defined. They had been magnetized with a concur magnetization directed along the

separation distance axis while the attraction force on the IPM center of mass had been measured at varying the separation distance.
The simulated separation distance between two facing surfaces had been ranged from 2 cm to 6 cm with an incremental step of 0.1 cm. Same mesh definition and similar computational time had been obtained. The data had been exported and analyzed in Matlab to calculate its regression.
The selected actuation unit PM underwent the same simulation to calculate their static attraction force (F_{Act}) that is used to define the structural model used to predict the weight that the device can support.

Motion

A Comsol multiphysics 3D simulation with the selected anchoring unit PM had been performed to calculate the dragging force (F_{drag}) and the attraction force (F_a) at varying the misalignment (m) along the x direction only, figure 1.26. The simulation had been performed using the same settings used for the attraction force calculation but with different EPM and IPM spatial configuration. Separation distance (d) had been kept constant to 3 cm while the misalignment distance (m) had been ranged from 0 cm to 3.75 cm with an incremental step of 0.0635 cm. None analysis had been performed about a z axes misalignment because is not the device axis thus the eventual dragging direction. The data were exported and studied in Matlab.
A static friction coefficient of the internal abdominal wall (μ_{abd}) of 0.1 had been reported by Loring et al. [50] and it had been used to calculated the resultant friction force (F_f).

Model

A 3D printed (Stratasys - Objet 30 Pro) device phantom that embeds the selected IPM had been built to verify the proposed model in a specific bench test. The

device phantom had been placed at a controlled separation distance (vertical slider) from the external coupler (see section 2.6) that embeds the two magnetic units EPM. An incremental known weight (F_W) had been hanged from the hinge point of the retracting lever until failure, rotation around the anchoring unit edge, occurred. Figure 2.24.

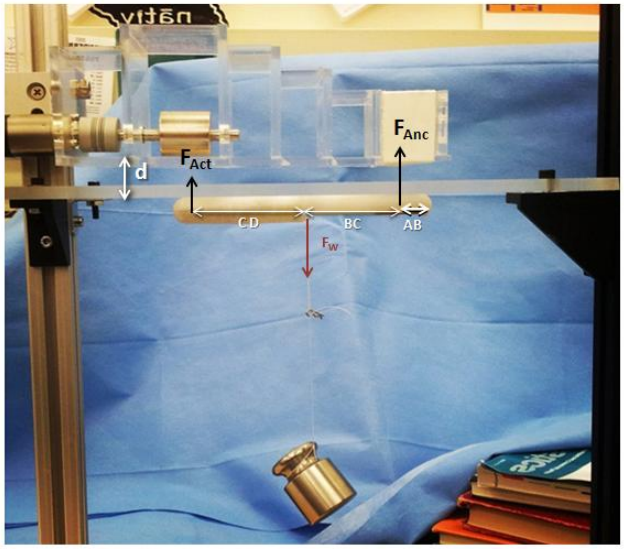

Figure 2.24: bench test utilized to validate the structural model of the device and thus predict the device unloading capacity at different separation distance.

The test had been performed varying:

- the separation distance d (thus varying the F_{Act} and F_{Anc} forces) from 2 cm to 4 cm with 0.5 cm step adjusting the outside the body coupler position with the use of a caliber.
- varying the AB length of the device, thus the forces lever, while maintaining constant the other lengths. In particular, different parts with different lengths that allow a range test of the described variable from 2 cm to 5 cm with a range of 0.5 cm had been 3D printed.

Three repetition for each separation distance and AB length had been performed.

The device phantom information listed in table 8 had been integrated in a model elaborated in Excel that, given equation 29, predicts the device unloading capacity for different separation distance and AB length.

Parameters	Value
AB	**[2; 2.5; 3; 3.5; 4; 4.5;5] cm**
BC	**5.625 cm**
CD	**5.625 cm**
Separation distance (d)	**[2; 2.5; 3; 3.5; 4] cm**
F_{Act} (d)	***See equation 31***
F_{Anc} (d)	***See equation 30***
Device phantom weight	**56.75 gr**
Actuation unit IPM weight	**4.77 gr**
Anchoring unit IPM weight	***See figure 2.25***

Table 2: input parameter of the structural model used to validate the structural model that allow the device weight support prediction

The resulting weight force of IPM had been subtracted to their relative attraction forces while the device phantom weight force had been assumed unloaded equally by the two unit.

Both the tests results and the model prediction at varying the AB length and the separation distance had been studied in Matlab.

2.2.3 ANCHORING UNIT - RESULTS

The selected couple of PM (figure 2.25) had been purchased (K&J Magnetics, Jaminson U.S.) and their characteristic are listed in table 3.

	EPM	IPM
X	25.4mm	38.1 mm
Y	25.4mm	6.375 mm
Z	25.4mm	6.375 mm
Brmax	14 800 Gauss	13 200 Gauss
Magnetization grade	N52	N42
Price	34.76 $	3.11$
Weight	122.9 gr	11.52 gr

Table 3: selected EPM and IPM of the anchoring unit

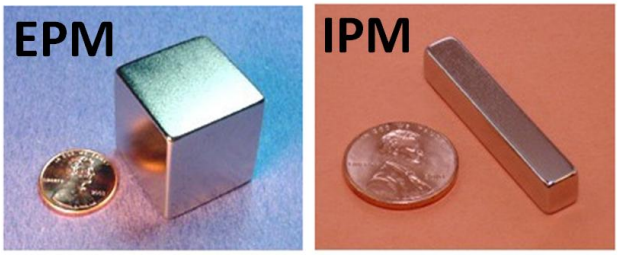

Figure 2.25 purchased anchoring unit couple of EPM and IPM (K&J Magnetics, Jaminson U.S).

The obtained attraction forces at varying the separation distance d, of both the anchoring unit and actuation unit are showed in figure 2.26 and their regression equation expressed in equation 30 and equation 31.

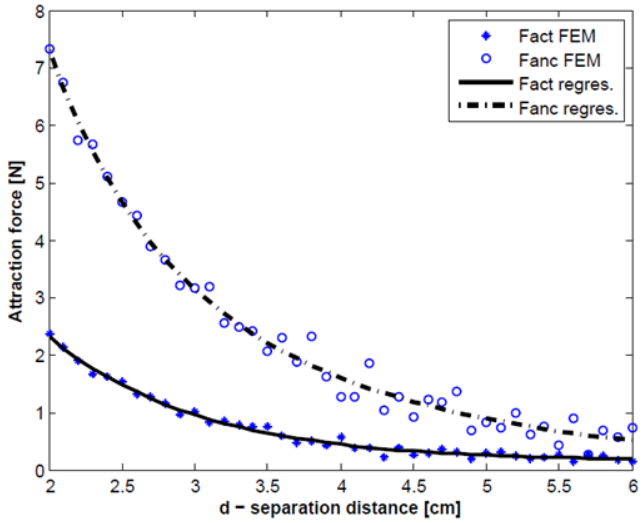

Figure 2.26: obtained attraction forces acting on the actuation unit IPM and anchoring unit IPM at varying the separation distance d.

$$F_{Anc}(d) = 66.92 \cdot e^{-1.538\,d} - 12.15 \cdot e^{-0.5286\,d} \quad (30)$$
$$F_{Act}(d) = 15.24 \cdot e^{-0.9621\,d} - 0.08611 \cdot e^{-0.08962\,d} \quad (31)$$

The force interested in the motion model (F_a, F_f and F_{drag}) at varying the misalignment (m) are showed in figure 2.27.

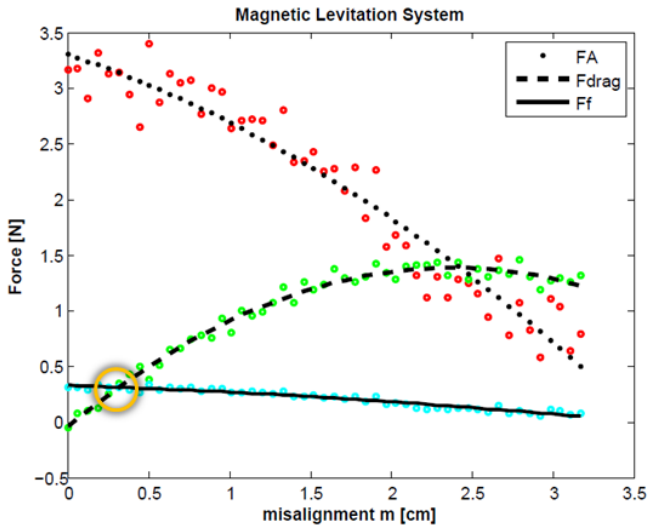

Figure 2.27: the simulated F_a, F_f and F_{drag} at varying the misalignment m and their 2-grade polynomial regression.

The IPM motion occurs when the F_{drag} force exceed the F_f one. This is achieved with a misalignment of 2.8 mm while the attraction force F_a can still provide a stable anchoring. Hence the selected couple of PM are able to ensure workspace exploration of the device in clinical relevant range of abdominal wall.

The model predictions and bench test results (held weight) are instead listed in table 4.

d\AB	2 cm	2.5 cm	3 cm	3.5 cm	4 cm	4.5 cm	5 cm
2 cm	*(505.3)* 481.6 ± 7.6	*(526.6)* 501.6 ± 2.8	*(545.4)* 518.3 ± 7.6	*(562.2)* 528.3 ± 7.6	*(577.2)* 541.6 ± 2.8	*(590.7)* 558.3 ± 10	*(603)* 566.6 ± 7.6
2.5 cm	*(300.9)* 278.3 ± 7.6	*(314.7)* 290 ± 5	*(326.9)* 303.3 ± 7.6	*(337.7)* 313.3 ± 7.6	*(347.4)* 320 ± 8.6	*(356.2)* 330 ± 8.6	*(364.1)* 335 ± 8.6
3 cm	*(176.7)* 146.6 ± 2.8	*(186.2)* 156.6 ± 2.8	*(194.7)* 165 ± 5	*(202.2)* 171.6 ± 5.7	*(208.9)* 180 ± 5	*(214)* 185 ± 5	*(220.46)* 188.3 ± 2.8
3.5 cm	*(99.7)* 88.3 ± 7.6	*(106.6)* 96.6 ± 7.6	*(112.7)* 103.3 ± 7.6	*(118.1)* 108.3 ± 7.6	*(123)* 113.3 ± 7.6	*(127.3)* 118.3 ± 7.6	*(131.3)* 120 ± 10
4 cm	*(50.9)* 45 ± 5	*(56.1)* 50 ± 5	*(60.6)* 55 ± 5	*(64.6)* 58.3 ± 5.7	*(68.2)* 63.3 ± 5.7	*(71.5)* 68.3 ± 5.7	*(74.4)* 70 ± 5

Table 4: The model prediction in brackets, underneath the mean and standard deviation of bench test results are showed at varying both the separation distance d and the AB length.

The supported weight exponentially decrease with the increase of the separation distance (as depicted in figure 2.26) and slightly increase with the increase of the AB lever length. The model always over estimate the actual holding capacity measured with the bench test results have. The mean error is 9.06 ± 4.37%. The error can be intended as composed by two components: an offset value given by the model overestimation of the attraction forces F_{Act} and F_{Anc} (that depends on the separation distance d), while a lower but more variable component that take in consideration the AB length variable.

2.5.4 ANCHORING UNIT - DISCUSSION

The selected PM have completely different shapes: a long IPM can exploit the device length that is occupied by the retracting lever and moreover offers a longer AB length which had been demonstrate to slightly increase the device holding capability. The EPM had instead been selected among the available one because of the higher grade of magnetization N52. A more flat EPM is advisable since it can offer a lower center of mass and thus higher attraction forces.

The selected anchoring unit, given the IPM dimension, can theoretically guarantee motion of the internal device inside the abdominal wall in clinical relevant abdominal thickness, it also never generates harmful stresses on the patient abdominal wall since the maximum pressure in the described range is 30.17 KPa.

The validated (mean error < 10%) structural model can be a useful tool, knowing the separation distance, to predict the retracting capacity of the device and avoid failure. The assumption of having constant attraction force acting on the Actuation unit IPM is a strong limitation of the model. The dynamical behavior and variation of the magnetization angle (θ_d and θ_D) cannot provide a static attraction force. Nevertheless this had been taken in consideration during the final tests procedure. Working conditions with a certain range of security from the predicted value had been tested (see section 3.2).
During the retraction procedure, the weight force increases with the closing up of the lever due to the increase of the displaced tissue and on the other hand, the weight force momentum decrease because of the lever closure.

2.6 ADDITIONAL COMPONENTS

Device Shell

All the device's component have to be contained in a 12 mm diameter device. The material has to be resistance and avoid breakage due to bending stresses caused by the counteraction of attraction forces of the anchoring unit and the tissue weight one. The device material has to be biocompatible and non toxic so that does not generate a inflammatory response in the abdominal cavity.

Knowing all the components dimensions and alignments the device body had been designed in Pro Engineering and 3D printed (Stratasys - Objet 30 Pro) in VeroWhite®+ material, Figure 2.28.

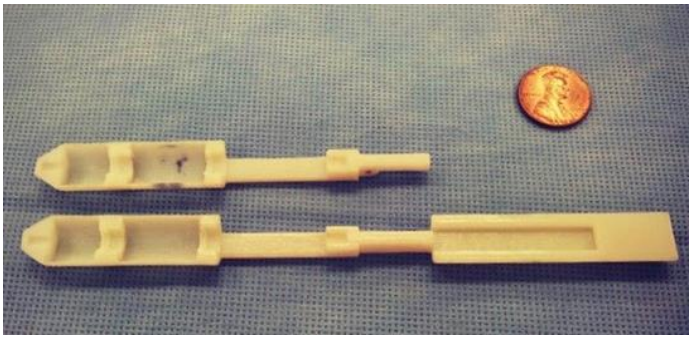

Figure 2.28: 3D printed device body halves.

An increase 12.5 mm diameter device shell had been obtained to compensate the poor mechanical properties of the fabrication material. To simplify the assembly procedure the device body had been divided in two halves kept together by a thin Parafilm® layer wrapped around.

Non Magnetic Bearing

Mechanical trains performance is badly influenced by misalignment problem of the components. Bearing guarantee optimal alignment and very low friction values. Because of the magnetic field interactions with commercially available

metallic bearing, non magnetic bearing that fit the small dimensions had been fabricated.

A 6 mm external diameter, 3 mm internal diameter and 3 mm thick Delrin ® bearings had been fabricated and coupled with the mechanical train shafts. Delrin offers high wear resistance and very low friction values.

External Coupler

The magnetic actuation and anchoring of the internal device is entrusted by the two selected EPM that must be embedded in an external controller. The external controller has to be designed as well. Example of external coupler for magnetically actuated devices have already been described for medical device with wireless magnetic actuations, as the RoboImplantII [51]. A laser cut ergonomic external coupler that embeds the two selected EPM, with the same separation distance that the two embedded IPM have, had been obtained from Plexiglas sheets. The actuation unit EPM had been connected with the use of a shaft coupler to a Falhauber 2342S024CR motor and maintained aligned thanks to purchased bearings. In figure 2.39 a three dimensional rendering and the corresponding 2D projections are showed.

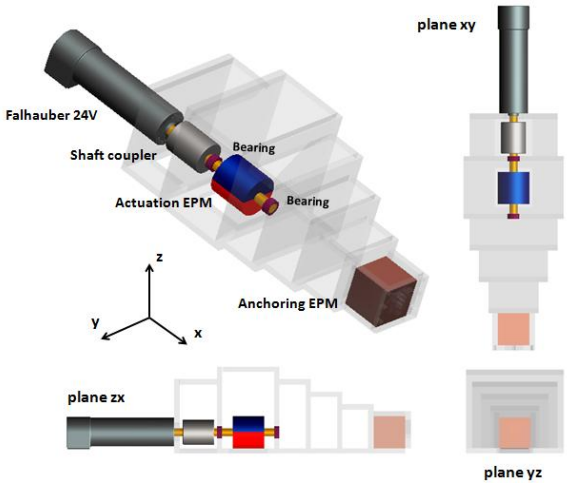

Figure 2.29: 3D rendering and corresponding 2D projection of the external coupler that embeds the two selected EPM.

3 THE LAPR-LMA

3.1 ASSEMBLED CONFIGURATION

The internal tissue retractor assembled is showed in figure 3.1 a, while the components described in section 2 are highlighted in figure 3.1 b, where the bottom half of the device shell had been removed.

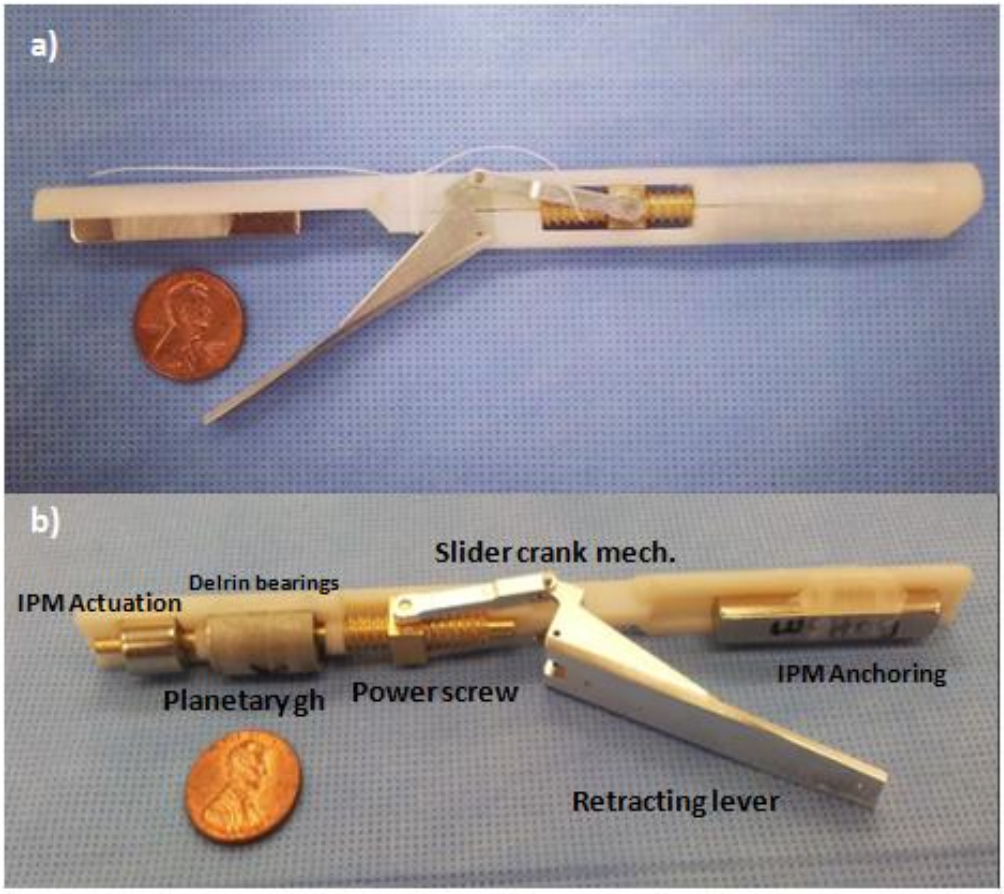

Figure 3.1: a) assembled designed internal tissue retractor. b) designed device where the bottom half of the body had been removed to show the studied and designed components.

LapR_LMA weights 39.16 g is 154 mm long and 12.5 mm in diameter.

3.2 DEVICE PERFORMANCE

Thanks to the previous components characterization is possible to compare at varying the separation distance the device performance (i.e. power transmission and attraction forces) during the retraction procedure (i.e. γ lever angular displacement) in terms of weight that can be retracted and stable hold by the device. From the comparison is possible to describe if the device functioning is stable and which of the two components (actuation or anchoring) can be improved or redesigned.

The retracting performance can be pointed out taking in consideration multiple information obtained during the analysis:

1. the transmittable torque of the actuation unit at varying the separation distance (equation 13).
2. the GR of the Planetary gearhead (64:1), its efficiency (61.24%) and the maximal safe transmittable torque (134.64 mNm) that the gears can transmit calculated with equation 17.
3. the power screw efficiency (69.85%) and the calculated mechanical transfer function β_{lead} (0.9117 N/mNm).
4. the offset crank mechanical advantaged Γ at varying the lever angle γ (equation 28) and the lever length (58.5 mm).
5. neglectable collar friction acting on the shafts due to the Delrin bearings.

The stable support of the weight can instead be predicted by the validated structural model (equation 29) at varying the separation distance taking in consideration that while the lever closes (γ) the mass that can be supported increase due to a lower arm of the weight force.

A graph where the separation distance is on the x axes while the retracted weight is expressed on the y axes can be built and offers the working range of

the device allowing the user to predict retracting capability. Failure can be defined as caused by an insufficient power transmission and thus torque at the lever tip, or by to an inadequate unloading performance, figure 3.2.

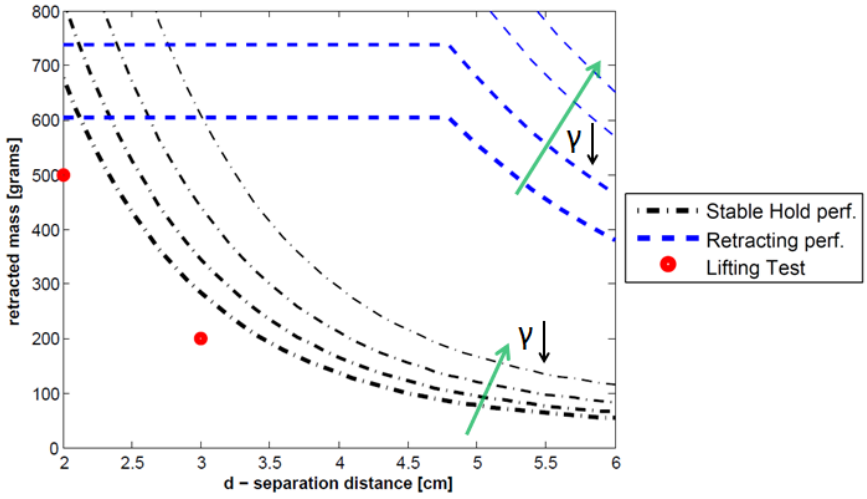

Figure 3.2: Device performance at varying the separation distance. In black: stable hold performance offered by the attraction forces, in blue: mechanical train retract performance. The working range is the area underneath both the two performance. Two lifting tests, expressed by the red dots, had been performed to verify the predicted device functioning.

The stable hold performance is showed in black and increase with the lever closing, the retract performance is instead represented in blue and as well increase with the lever closure.

From the graph is clear that the actuation unit and the designed mechanical train can retract any weight that can be supported by the anchoring unit even if the planetary gearhead impose a torque limitation in the transmittable power. Because of the performance difference between the mass that can be retracted and the one that can be supported, the anchoring unit results under estimated.

Nevertheless the mechanical gear train designed is theoretically able, assuming an optimal stable hold performance, to retract more than 600 grams in a range of abdominal thickness that include obese patients (BMI > 30kg/m^2).

To verify the predicted performance and test the device behavior and functioning two lifting test, showed by the two green dots in the working range of figure 3.2, had been set up and are described in section 3.3.1.

3.3 TEST

3.3.1 QUANTITATIVE VALIDATION

The insertable device had been placed at 2 cm of distance from the external controller, 500 grams had been hanged from the lever tip in a fully open configuration (γ= 90°) and retracted until the retracting lever angle γ reached a closed configuration. The device had been fed with an actuation unit velocity of 1700 RPM.

A second test where the separation distance had been fixed at 3 cm and 200 grams had been hanged to the open retracing lever had been performed with the actuation speed and the retraction performed until lever closure.

In figure 3.3 a series of snapshot of the video that document the first test are showed.

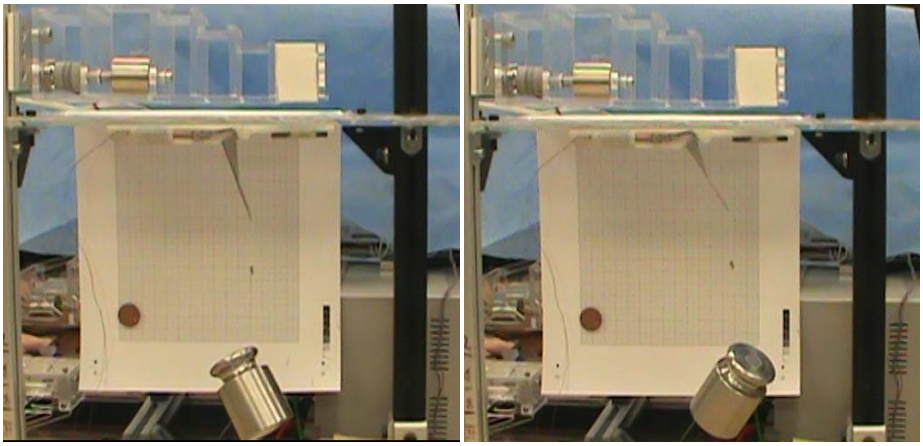

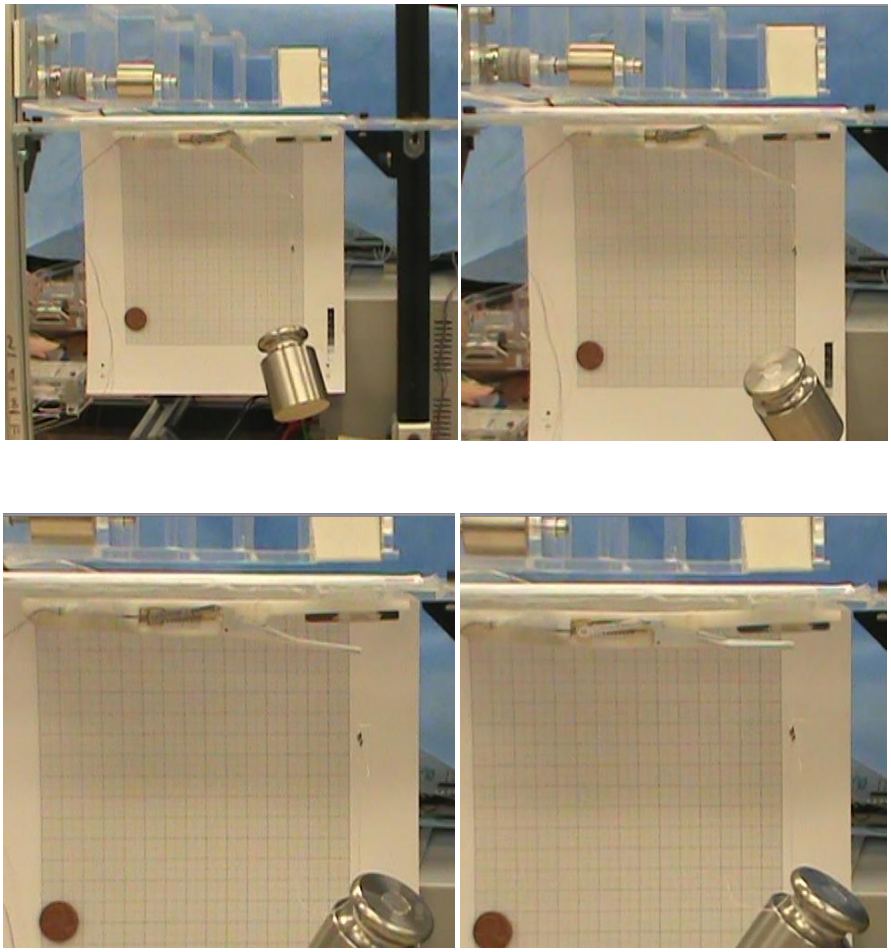

Figure 3.3: series of snapshot of the video that document the retracting test with 500 grams.

In both cases the retraction had been performed successfully and once performed and the power transmission had been stopped. The maintenance of the retracted weight had been guaranteed by the PS-nut non back drivability.

As visible from the last pictures, when fully retracting 500 grams, the device body is bended by the momentum generated at the lever hinge point. Thus the proposed arrangement of the mechanical components results more reliable than having them inside a thin outer layer device body.

3.3.2 QUALITATIVE VALIDATION EX VIVO

The device had also been tested to qualitatively analyze the retraction solution proposed. Ex vivo tests had been performed retracting a two lobes pig liver (total weight 672 grams). The pig liver had been placed at about 15 cm of distance from the simulated abdominal wall (rigid Plexiglas sheet) to simulate the inflated abdominal cavity. A gripper, wired to the lever tip, had been used to clutch a single lobe edge. The device placed at 2 cm (figure 3.4 a) and 4 cm (figure 3.4 b) of distance from the external controller had been actuated with an actuation unit speed of 1700 RPM and the retraction performed.

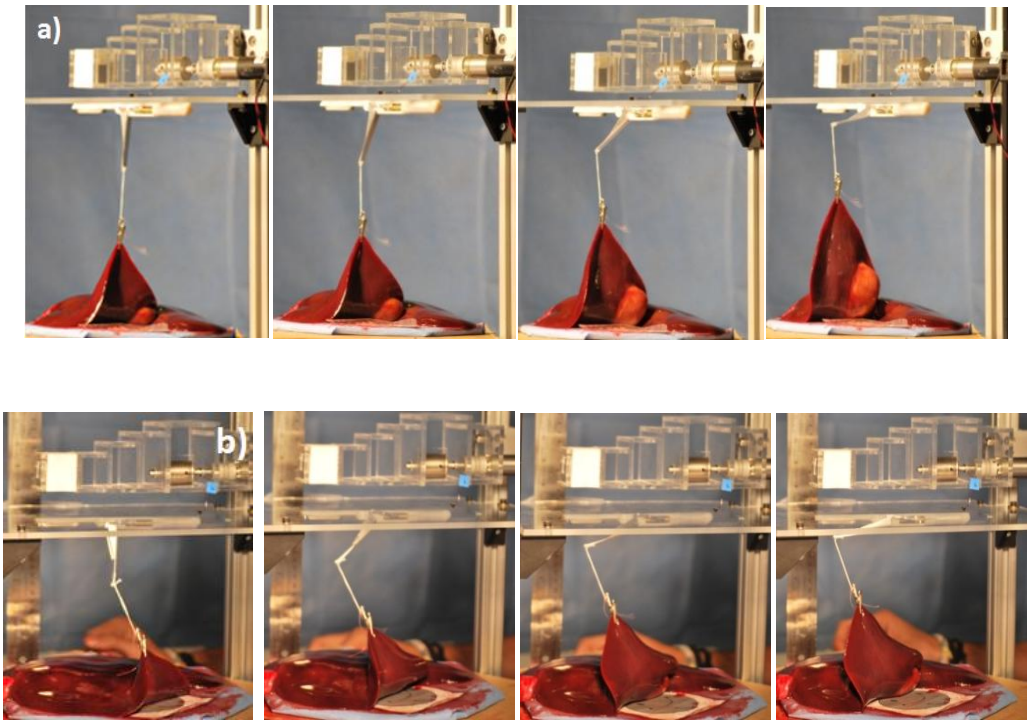

Figure 3.4: a) sequence of snapshot that document the retraction of a pig liver lobe with a simulated abdominal thickness of 2cm. The gallbladder is well exposed. b) sequence of snapshot that document the retraction of the same lobe but with a simulated abdominal thickness of 4 cm.

In both cases the retraction had been successfully performed and no failure occurred. As depicted in the series of snapshot of figure 3.4 a, the gallbladder

that laid under the retracted lobe is exposed thus the retraction solution can be considered valid.

4 DISCUSSION

A Laparoscopic tissue retractor based on a new approach for medical robotic called Local Magnetic Actuation had been designed, fabricated, characterized and tested. The insertable device is magnetically coupled with and external coupler and results 12.5 mm in diameter, 154 mm long and weights 39.16 grams.

The achieved technical specification can be pointed out with respect of the clinical requirements described in section 1.6:

1) the device can be moved and actuated (section 2.5.4 and section 2.1.4 respectively) in a range of relevant abdominal thickness that include obese patients.
2) the device is able to enter the abdominal wall through standard trocar of 12 mm (they in fact normally have tolerances up to 2 mm).
3) A pig liver (672 grams) had been successfully retracted with a simulated abdominal thickness of 4 cm. The mechanical gear train had been able to lift to 500 grams at 2 cm. From the device performance (figure 3.2) the device results able to retract the same weight with a simulated abdominal thickness up to 4.6 cm. The anchoring performance results underestimated and cannot support such a high weight in the same range of abdominal thickness. Nevertheless the modularity of the device permits to interchange its components and predict its functioning in a fast and reliable method. From the ex vivo test is clear that the actual weight of the target organ is not the felt weight that the device feels during the retraction. Thus 750 g cannot be lifted but might be retracted.

4) The anchoring unit never generate potentially damaging compression stresses on the patient abdominal wall. In order to satisfy this requests and increase the anchoring performance that result limiting, more powerful PM couple can be selected and a control strategy adopted to control attraction force acting on the IPM. The anchoring unit EPM can be placed further away from the patient belly and controlling its position, approached to generate higher attraction forces on the IPM only during the retraction procedure. In this way a higher stable performance is guaranteed and potentially damaging compression stresses balanced by the retracted weight force that decrease the pressure acting on the abdominal wall.
5) A controllable internal degree of freedom actuated magnetically is able to generate, in a range of abdominal wall thickness that include obese patients, forces at the end effector tip, higher than 6 N (figure 3.2). The retraction procedure (i.e. 90° spawn of the retracting lever) takes 18.17 sec.
6) The device can explore the abdominal workspace and be placed in optimal position for retracting as demonstrated by the motion analysis in section 2.5.3. This ensure a reduced encumbrance of the endoscopic view and an optimal positioning of the device that can avoid interference with other surgical instrumentations.
7) The internal device contains only passive components but the selected PM magnetic properties fade if the temperature exceed 80 °C. Nevertheless the supplier guarantee the possibility to treat PM to make the resistant up to 200° C thus allowing the use of autoclave to sterilize the internal device.

The device functioning had been demonstrated reliable, secure and stable due to the increase of performances with the lever closure. The mechanical power in

term of torque, that can be transferred to an on board PM had been quantified and demonstrated to be higher than commercially available micro motors.

5 CONCLUSION AND FUTURE DEVELOPMENT

The obtained device is the first version of a first magnetically actuated-anchored internal surgical device based on LMA. Its functioning had been described, the components characterized, performance predicted and verified with tests.

In order to better describe the mechanical train behavior analyzing its losses and more solidly determine the working range of the device, lifting weight tests where the input power of the system (i.e. actual transmitted torque) is measured, can be tested. The actuation unit IPM magnetization angle (θ_d) can in fact be recorded with a magnetic field sensor (Hall Effect Sensor Element CY-P15A) and comparing it with the EPM magnetization angle (θ_D), determine the effective transmitted torque (equation 1) necessary to lift a known weight.

Ex vivo test on porcine or sheep model in surgical environment should be performed to check the device insertion and functioning inside an inflated abdominal cavity and to receive feedback the surgeons regarding device dimensions and retraction solution.

From the ex vivo tests, it results necessary to investigate how the displacement of internal tissues is translated in felt retracted weight so that the device performance can be shifted to a retraction scenario rather than a lifting one.

An optimized second version can then be developed taking in consideration the con's of the designed device:

- A more powerful anchoring unit can be sized

- The device body can be fabricated in a more resistance and biocompatible material to satisfy that the 12 mm requirement.
- The designed mechanical components can be better designed taking in consideration the each component discussion (section 2.X.5) and their mechanical resistance better analyzed with analysis of the internal stresses.

To investigate the feasibility of the LMA approach for surgical robotic devices that include multiple actuation unit and thus multiple DoF device, future direction has to be directed in studying magnetic interaction phenomena. For LapR_LMA in fact the two magnetic unit had been characterized as completely uncoupled but the author reports a possible disruptive magnetic interaction between the two units if their separation distance was radically decreased.
Is necessary to define limit distances between the different unit and optimized the EPM dimensions. Magnetic shielding material are an interesting possible investigation [52].

BIBLIOGRAPHY

[1] F. Herrel et al. “Minimally invasive abdominal surgery: Lux et veritas past, present, and future” Am J Surg; 190(2): 239-43, 2010.

[2] J. Varela et al. “Laparoscopic surgery significantly reduces surgical-site infections compared with open surgery” Surgical Endoscopy, 24(2):270-276, 2010.

[3] M. Boltz et al. “Hospital costs associated with surgical site infections in general and vascular surgery patients” Surgery, 150(5): 934-942, 2011.

[4] J. Fuller et al. “Laparoscopic trocar injuries: A report from a U.S. Food and Drug Administration (FDA) Center for Devices and Radiological Health (CDRH) Systematic Technology Assessment of Medical Products (STAMP) committee”, 2003. www.fda.gov/medicaldevices/safety/alertsandnotices/ucm197339.htm.

[5] M.M. Lerici et al. “Single site laparoscopic surgery: An intermediate step toward no (visible) scar surgery or the next gold standard in minimally invasive surgery?” MITAT, 21(1):1:7, 2012

[6] P.Strickland et al.”Transvaginal natural orifice translumenal endoscopic surgery (NOTES): a survey of women’s views on a new technique” Surg Endosc.;24(10):2424-31, 2010

[7] J.R. Romanelli “Single port laparoscopy: an overview” Surg Endosc.;23(7):1419-27, 2009

[8] A. Schill et al. “Comparison of laparoscopic skills performance between singlesite access (SSA) devices and an independent-port SSA approach” Surg Endosc;26(3):714-21, 2012

[9] M.E.Rentschler et al. “Natural orifice surgery with an endoluminal mobile robot” Surg Endosc.;21(7):1212-1215, 2007

[10] G. Haber et al. “Novel robotic Da Vinci instruments for laparoendoscopic single-site surgery”. Urology, 76(6):1279-1282, 2010.

[11] R.A.Beasley et al. “Medical Robots: Current Systems and Research Directions” Journal of Robotics, (2012) Article ID 401613, 2012

[12] J. Ding et al. “Design, Simulation and Evaluation of Kinematic Alternatives for Insertable Robotic Effectors Platforms in Single Port Access Surgery” in Proc. of IEEE International Conference on Robotics and Automation (ICRA) 2010.

[13] M.J.H. Lum et al.“The RAVEN: Design and Validation of a Telesurgery System” J of Robotics vol. 28 no. 9 1183-1197, 2009

[14] C. Di Natali et al.“Trans-abdominal Active Magnetic Linkage for Robotic Surgery: Concept Definition and Model Assessment”, in Proc. of IEEE International Conference on Robotics and Automation (ICRA) 2012, St Paul, MN, USA, 2012

[15] T. Ranzani et al.“A Novel Surgical Robotic Platform Minimizing Access Trauma”, in Proc. of 4th Hamlyn Symposium on Medical Robotics, London, UK, pp. 15-16. 2011

[16] C. Di Natali et al.“Remote active magnetic actuation for a single-access surgical robotic manipulator”, in Proc. of the XVI Annual Conference of the International Society for Computer Aided Surgery (ISCAS) 2012, Pisa, Italy, 2012.

[17] http://www.covidien.com/covidien/pages.aspx

[18] http://www.virtual-ports.com/default.asp

[19] B.E.Padilla et al. “The use of magnets with single-site umbilical laparoscopic surgery” Seminars in Pediatric Surgery, 20(4), 224-234, 2011

[20] Y.B.Cho et al. “Transvaginal endoscopic cholecystectomy using a simple magnetic traction system” Minimally Invasive Therapy ; 18(4), 1–5, 2010

[21] M.Kume et al. “The use of magnetic anchors in the bowel lumen for laparoscopic anterior resection of rectosigmoid colon in pigs: with video.” World J Surg.;32(11):2425-2428. 2008

[22] G. Tortora et al. “Array of Robots Augmenting the Kinematics of Endocavitary Surgery”, IEEE Transactions on Mechatronics (TMech),PP (99), 2014

[23] D.Canes et al. “The future of NOTES instrumentation: Flexible robotics and in vivo minirobots.” J Endourol. ;23(5):787-92, 2009

[24] S.Park et al. “Trocar-less instrumentation for Laparoscopy” Ann Surg.; 245(3): 379–384. 2007

[25] I.S.Zeltser et al. “Single Trocar Laparoscopic Nephrectomy Using Magnetic Anchoring and Guidance System in the Porcine Model” The Journal of Urology, 178(1), 288-291; 2007

[26] M. Cadeddu et al.”Retraction force measurement during transgastric and transvaginal NOTES”. Gastrointestinal Endoscopy, 67(5):AB119, 2008.

[27] B. Padilla, et al. “The use of magnets with single-site umbilical laparoscopic surgery”. In Seminars in Pediatric Surgery, volume 20, pages 224-231, 2011.

[28] M. Ryou et al. “Magnetic retraction in natural-orifice transluminal endoscopic surgery (NOTES): addressing the problem of traction and countertraction”. Endoscopy, 41(2):143-148, 2009.

[29] S.L. Best et al. “Maximizing coupling strength of magnetically anchored surgical instruments: how thick can we go?” Surg Endosc.;25(1):153-9, 2011

[30] T. Hu et al. “Insertable Surgical Imaging Device with Pan, Tilt, Zoom, and Lighting” The International Journal of Robotics Research; 28; 1373, 2009

[31] D.K. Molina et al. “Normal organ weights in men: part II-the brain, lungs, liver, spleen, and kidneys” Am J Forensic Med Pathol., 33(4):368-72,2012

[32] S.L. Best et al. “Magnetic Anchoring and Guidance System Instrumentation for Laparo-endoscopic Single-site Surgery/Natural Orifice Transluminal Endoscopic Surgery: Lack of Histologic Damage After Prolonged Magnetic Coupling Across the Abdominal Wall” j. urology, 5 (041), 2010

[33] M. Piccigallo et al. “Design of a Novel Bimanual Robotic System for Single-Port Laparoscopy” Mechatronics IEEE, 15(6), 871-878, 2010

[34] E.P. Furlani “Permanent Magnet and Electromechanical Devices: Materials, Analysis, and Applications” Elsevier 2001

[35] E.P. Furlani “Analytical analysis of magnetically coupled multipole cylinders” J. Phys. D: Appl. Phys. 33 28, 2000

[36] M. Simi et al. “Magnetic Levitation Camera Robot for Endoscopic Surgery” Robotics and automation, ICRA 2011 International conference, Shanghai, 2011

[37] M. Simi et at. “Magnetic Torsion Spring Mechanism for a Wireless Biopsy Capsule” ASME J MED, 7(4), 2013

[38] R.G. Montague et al. “Magnetic Gear Pole-Slip Prevention Using Explicit Model Predictive Control” Mechatronics IEEE, 18(5), 1535-1543, 2013

[39] R.G. Montague “Servo control of magnetic gears” Mechatronics IEEE, 17(2), 269-278, 2012

[40] F. Roos et al. “Optimal selection of motor and gearhead in mechatronic applications” Mechatronics 16(1) , 63–72, 2006

[41] I. Usitalo et al. “Mini assembly cell for the assembly of mini-sized planetary gearheads” Assembly Automation ; 24(1):94-101, 2004

[42] A.B. Rathod "A parametric modeling of spur gear using ProEngineer" National Conference on Recent Trends in Engineering & Technology, 2011

[43] A. Stokes "Gear handbook design and calculations" Butterworth-Heinemann 1992

[44] J. Shigley "Standard Handbook of Machine Design" Mc Graw Hill, 2004

[45] J.A. Collins "Mechanical design of machine elements and machines" John Wiley & Sons, 2010

[46] M.A. Chowdhury "Friction Coefficient of Different Material Pairs Under Different Normal Loads and Sliding Velocities" Tribology in industry, 34(1), 18-23, 2012

[47] P. Burton "Kinematic and dynamics of planar machinery" Prentice-Hall, 1979

[48] O. Vinogradov "Fundamental of kinematic and dynamics of machines and mechanisms" CRC Press, 2000

[49] S.A. Janhavi "A study of scaling and geometry effects on the forces between cuboidal and cylindrical magnets using analytical force solutions" J. Phys. D: Appl. Phys. 41, 2008

[50] S.H.Loring et al. "Lubrification refimes in mesothelian sliding" J of Biomechanics 38(12) 2390-2396, 2005

[51] J.A.Liu et al. "ROBOImplant II: Development of a Noninvasive Controller/Actuator for Wireless Correction of Orthopedic Structural Deformities" 2012 ASME J MED 6(1), 2012

[52] R.D.Brewer et al. "Force Control of a Permanent Magnet for Minimally-Invasive Procedures" Conference on Biomedical Robotics and Biomechatronics Scottsdale, AZ, USA, October 19-22, 2008

APPENDIX: planetary gear head technical sheets

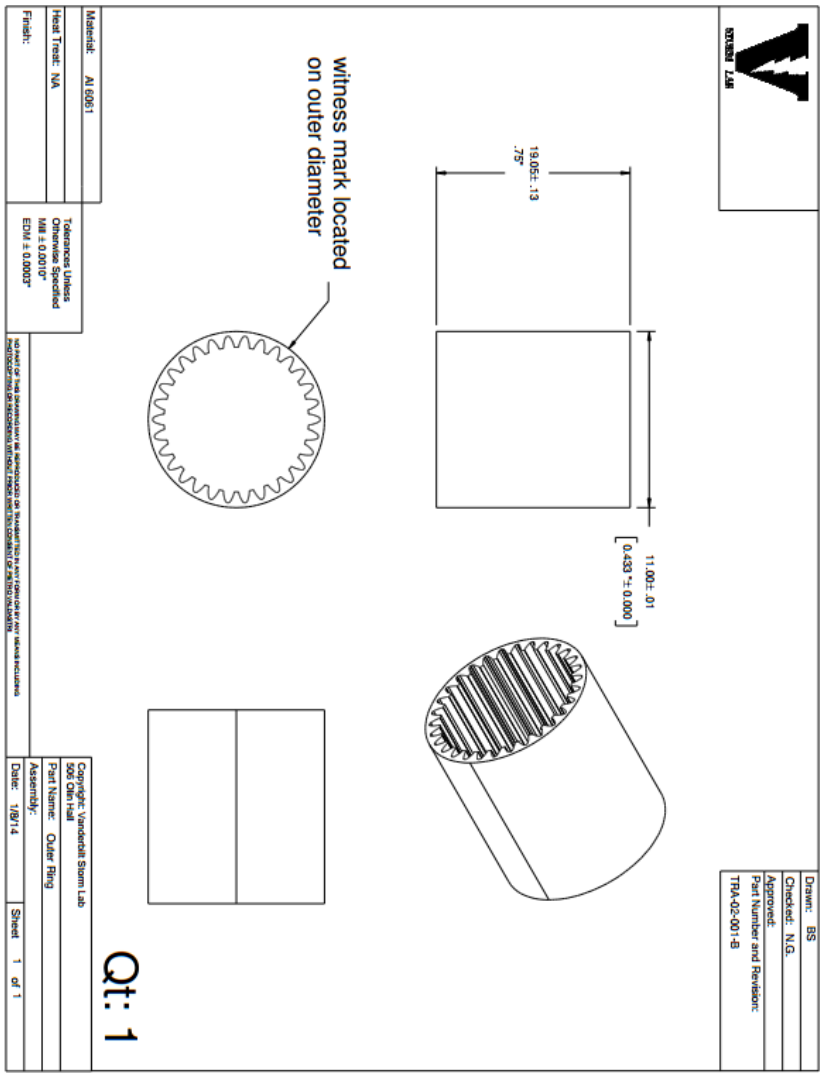

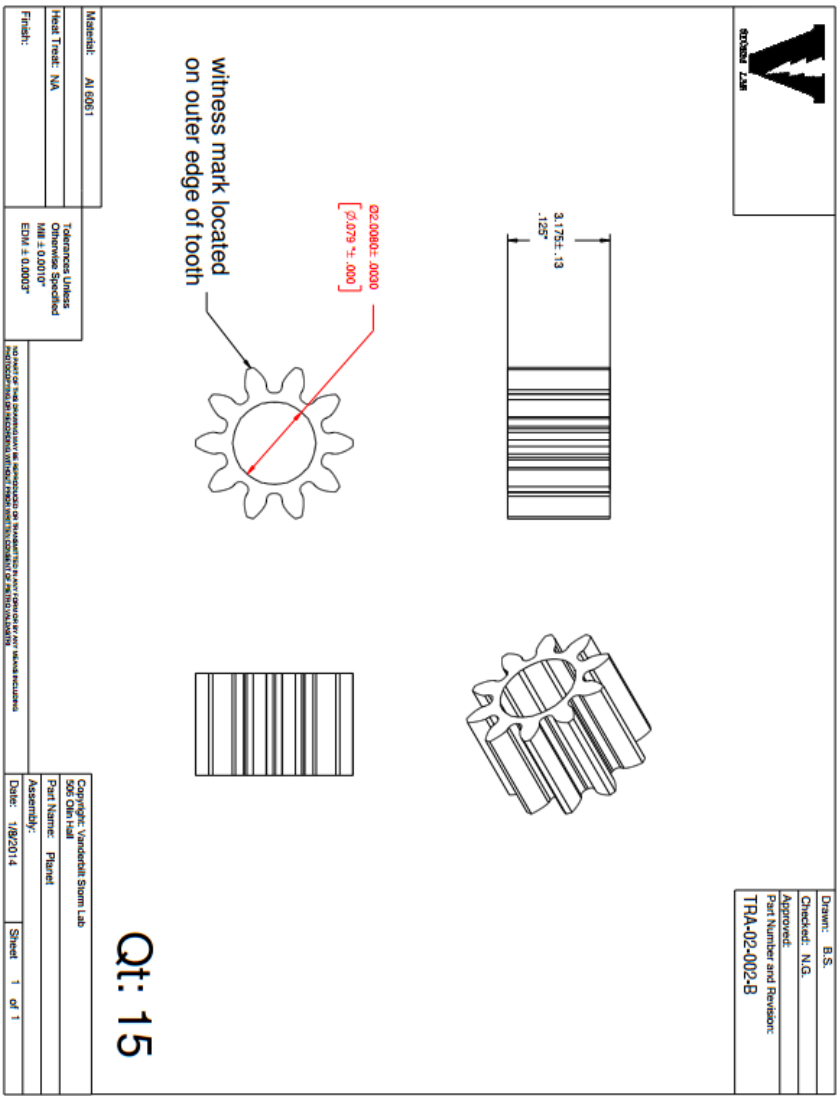
Drawn: B.S.
Checked: N.G.
Approved:
Part Number and Revision:
TRA-02-002-B
3.175± .13
.125"
Ø2.0080± .0030
[Ø.079 +± .000]
witness mark located
on outer edge of tooth
Qt: 15
Material: Al 6061
Heat Treat: NA
Finish:
Tolerances Unless
Otherwise Specified
Mill ± 0.0010"
EDM ± 0.0003"
Copyright: Vanderbilt Storm Lab
506 Olin Hall
Part Name: Planet
Assembly:
Date: 1/9/2014
Sheet 1 of 1

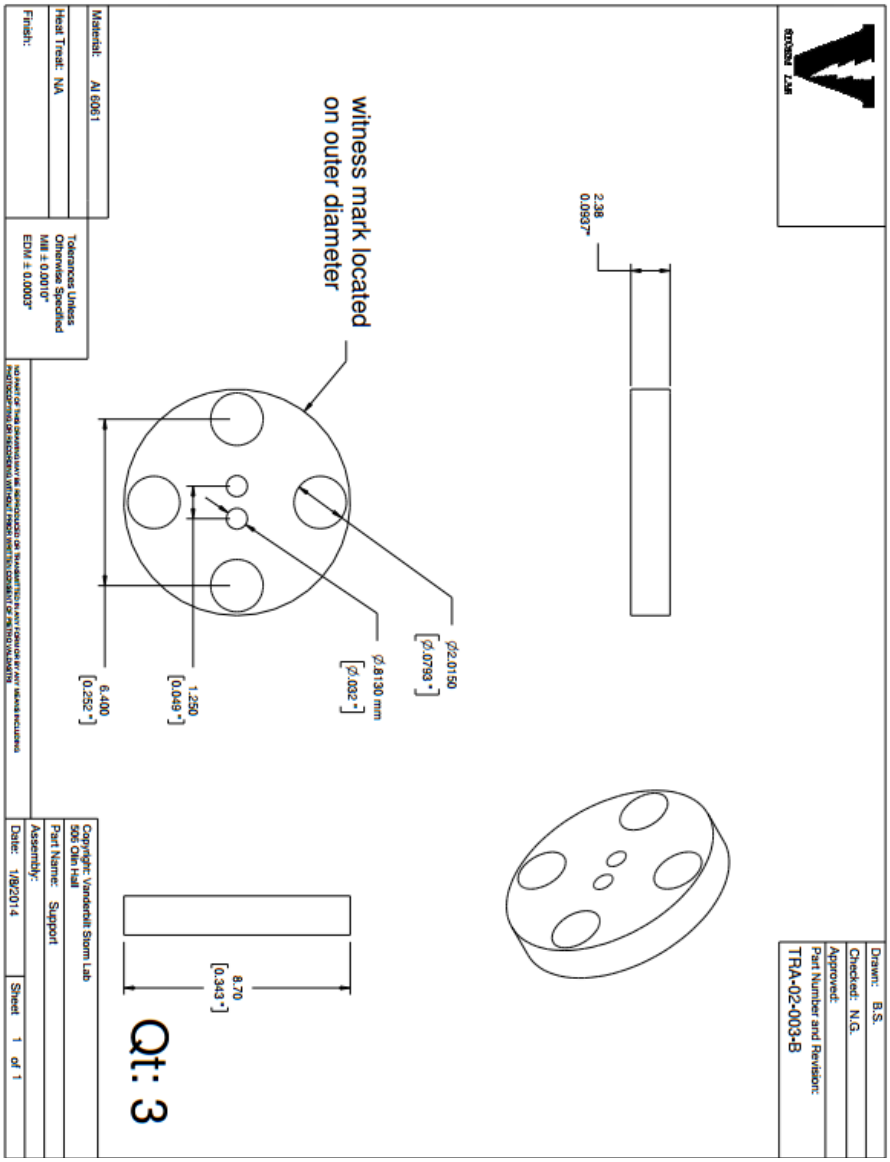
Drawn: B.S.
Checked: N.G.
Approved:
Part Number and Revision:
TRA-02-003-B
2.38
0.093"
witness mark located
on outer diameter
Ø2.0150
[Ø.0793"]
Ø.8130 mm
[Ø.032"]
1.250
[0.049"]
6.400
[0.252"]
8.70
[0.343"]
Qt: 3
Material: Al 6061
Heat Treat: NA
Finish:
Tolerances Unless
Otherwise Specified
Mill ± 0.0010"
EDM ± 0.0003"
Copyright: Vanderbilt Storm Lab
508 Olin Hall
Part Name: Support
Assembly:
Date: 1/8/2014
Sheet 1 of 1

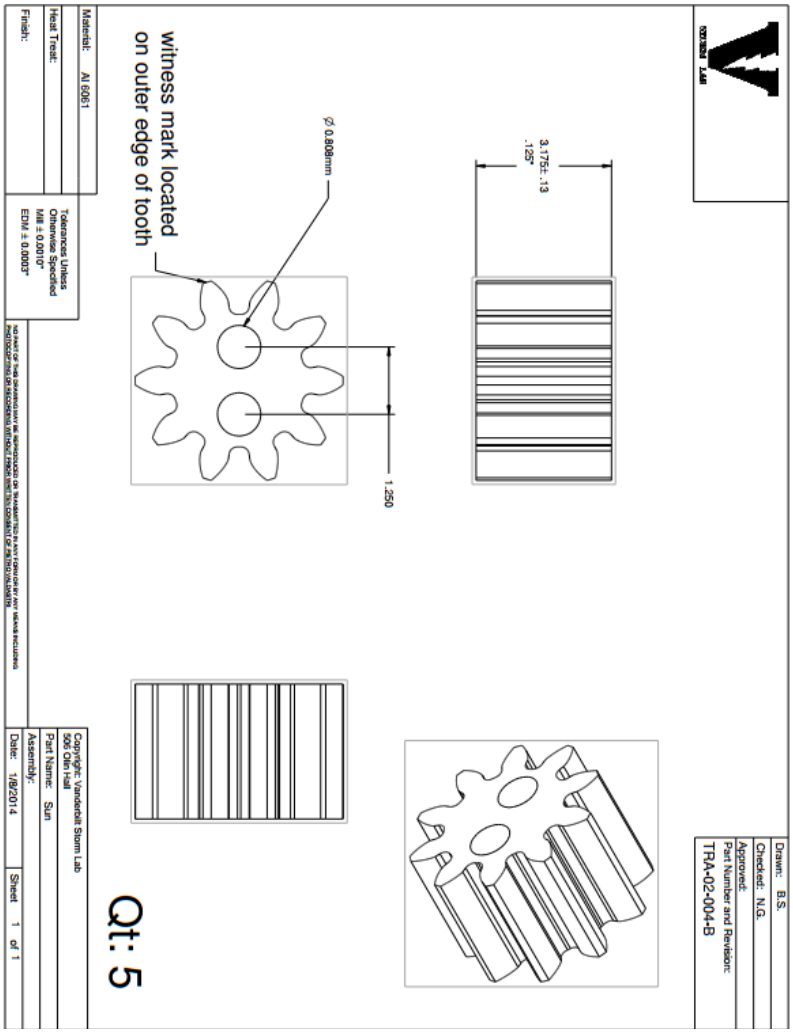
Drawn: B.S.
Checked: N.G.
Approved:
Part Number and Revision:
TRA-02-004-B
3.175± .13
.125"
witness mark located
on outer edge of tooth
Ø 0.808mm
1.250
Qt: 5
Material: Al 6061
Heat Treat:
Finish:
Tolerances Unless
Otherwise Specified
Mill ± 0.0010"
EDM ± 0.0003"
Copyright: Vanderbilt Storm Lab
506 Olin Hall
Part Name: Sun
Assembly:
Date: 1/8/2014
Sheet 1 of 1

Matlab Code

```
clear all;
close all;
clc;

% ACTUATION UNIT TORQUE ANALYSIS
TEST=importdata('IPM.txt');
distance=100*TEST(:,1);
ipm1=TEST(:,2);
ipm2=TEST(:,3);
ipm=-(ipm1+ipm2)/2;
plot(distance,ipm,'ro','LineWidth',1.5,'markersize', 5)
[curve2] = fit( distance, -ipm, 'exp2');
piccolo=-curve2.a .* exp(curve2.b.*distance(:))-curve2.c .*
exp(curve2.d.*distance(:));
hold on
plot(distance,piccolo,'LineWidth',2)
xlabel('h - separation distance [cm]','FontWeight','bold')
ylabel('torque [mNm]', 'FontWeight','bold')
title('Transmittable torque - LMA', 'FontWeight','bold')
%%
%attraction forces analysis
TEST2=importdata('attrazione.txt');
separation=100*TEST(:,1);
LMAipm=TEST2(:,2);
ANCipm=TEST2(:,3);
%LMA regression
[curve3] = fit( separation, LMAipm, 'exp2');
lma=curve3.a .* exp(curve3.b.*separation(:))+curve3.c .*
exp(curve3.d.*separation(:));
%anchoring regression
[curve4] = fit( separation, ANCipm, 'exp2');
anchoring=curve4.a .* exp(curve4.b.*separation(:))+curve4.c .*
exp(curve4.d.*separation(:));
figure
maybe(1)=plot(separation,LMAipm,'ro','LineWidth',1.5,'markersize
', 5);
hold on
maybe(2)=plot(separation,ANCipm,'go','LineWidth',1.5,'markersize
', 5);
maybe(3)=plot(separation,lma,'LineWidth',2);
maybe(4)=plot(separation,anchoring,'k','LineWidth',2.5);
xlabel('Separation distance [cm]')
ylabel('Attraction force [N]')
title('Attraction forces regression', 'FontWeight','bold')
legend([maybe],'LMA FEM','Anchoring FEM','LMA
regres.','Anchroing regres.','Location','NorthEast')
%%
% magnetic levitation system
TEST3=importdata('MagneticLevitationSystem.txt');
m=TEST3(:,1);
```

```
FA=TEST3(:,2);
Fdrag=TEST3(:,3);
Ff=TEST3(:,4);
%FA regression
[c1] = fit( m, FA, 'poly2');
FAA=c1.p1*m.^2 + c1.p2.*m + c1.p3
%c1.a .* exp(c1.b.*m(:))+c1.c .* exp(c1.d.*m(:));
%Fdrag
[c2] = fit( m, Fdrag, 'poly2');
Fdragg=c2.p1.*m.^2 + c2.p2.*m + c2.p3;
%Ff regression
[c3] = fit( m, Ff, 'poly2');
Fff=c3.p1.*m.^2 + c3.p2.*m + c3.p3;
figure
plot(m,FA,'ro','LineWidth',1.5,'markersize', 4);
hold on
plot(m,Fdrag,'go','LineWidth',1.5,'markersize', 4);
plot(m,Ff,'co','LineWidth',1.5,'markersize', 4);
maybe(1)=plot(m,FAA,'k.','LineWidth',2);
maybe(2)=plot(m,Fdragg,'k--','LineWidth',2.5);
maybe(3)=plot(m,Fff,'k','LineWidth',2);
xlabel('misalignment m [cm]', 'FontWeight','bold')
ylabel('Force [N]', 'FontWeight','bold')
title('Magnetic Levitation System', 'FontWeight','bold')
legend([maybe],'FA','Fdrag','Ff','Location','NorthEast')
%%
% OFFSET CRANK MECHANISM
% Displacemente analysis


%INPUT: position of the joint
O=[0,0]';
A=[5,8]';
B=[25,4]';
AO=A-O;
AB=B-A;
%offset and linear vector
s=B(1)-O(1);
e=B(2)-O(2);
%find angle and lenght
teta1=(atan(A(2)/A(1)));
teta2=(atan((B(2)-A(2))/(B(1)-A(1))));
%known position that moves with constant velocity
velocitamot=1500; %RPM
omegalead=velocitamot/(64*60); % giri al sec
pitch=1.5875; % mm
vlead=pitch*omegalead; %[mm/sec]
%range=13.4766;
range=12.7;
timereq=12.7/vlead;
num=100;
```

```
SRANGE=linspace(B(1),B(1)-range,num);
lAO=sqrt(A(1)^2+A(2)^2);
lAB=sqrt((B(1)-A(1))^2+(B(2)-A(2))^2);
Amove=[];
Bmove=[];

for i=1:num
    TETTA(i)=2*atan((-2*lAO*e - sqrt ( (-2*SRANGE(i)*lAO)^2 + (-
2*lAO*e)^2 - (SRANGE(i)^2+e^2+lAO^2-lAB^2)^2))/(-2*SRANGE(i)*lAO
- SRANGE(i)^2 - e^2 - lAO^2 + lAB^2));
    PHI(i)=2*atan((-2*lAB*e + sqrt ( (-2*SRANGE(i)*lAB)^2 + (-
2*lAB*e)^2 - (SRANGE(i)^2+e^2+lAB^2-lAO^2)^2))/(-2*SRANGE(i)*lAB
- SRANGE(i)^2 - e^2 - lAB^2 + lAO^2));

   % PHI(i)=atan((lAO*sin(TETTA(i))+e)/(SRANGE(i)-
lAO*cos(TETTA(i))));
    Axmove(i)= lAO*cos(TETTA(i)) ;
    Aymove(i)= lAO*sin(TETTA(i)) ;
    Bxmove(i)=[SRANGE(i)];
    Bymove(i)= [ B(2) ];
    DELTA(i)=pi+atan((Aymove(i)-Bymove(i))/(Axmove(i)-
Bxmove(i)));

end

%Velocity
VPHI=diff([PHI]);
VTETTA=diff([TETTA]);
VS=diff([SRANGE]);

%Accelleration
APHI=diff([VPHI]);
ATETTA=diff([VTETTA]);
AS=diff([VS]);

%plot position
figure
subplot(3,1,1)
plot(radtodeg(TETTA),'+')
subplot(3,1,2)
plot(radtodeg(PHI),'g*')
subplot(3,1,3)
plot(SRANGE,'ro')
%plot velocity
figure
subplot(3,1,1)
plot(VTETTA,'+') %[rad/sec]
subplot(3,1,2)
plot(VPHI,'g*') %[rad/sec]
subplot(3,1,3)
```

```
plot(VS,'ro')
axis([0 num -1 1])
%plot acceleration
figure
subplot(3,1,1)
plot(ATETTA,'+') %[rad/sec^2]
subplot(3,1,2)
plot(APHI,'g*') %[rad/sec^2]
subplot(3,1,3)
plot(AS,'ro')
axis([0 num -1 1])

%[SRANGE' radtodeg(TETTA') radtodeg(PHI')];
apertura=radtodeg(TETTA(num)-TETTA(1))

Amove=[Axmove' Aymove'];
Bmove=[Bxmove' Bymove'];

ii=linspace(1,length(Axmove),10);
 %
figure
for i=1%ii

plot ([O(1) Axmove(i)],[O(2) Aymove(i)], 'r','linewidth',3 )
hold on
plot ([-2.5+Bxmove(i) 2.5+Bxmove(i) ],[1.5+Bymove(i)
1.5+Bymove(i) ],'b','linewidth',3);
plot ([-2.5+Bxmove(i) 2.5+Bxmove(i) ],[-1.5+Bymove(i) -
1.5+Bymove(i) ],'b','linewidth',3);
plot ([-2.5+Bxmove(i) -2.5+Bxmove(i) ],[1.5+Bymove(i) -
1.5+Bymove(i) ],'b','linewidth',3);
plot ([2.5+Bxmove(i) 2.5+Bxmove(i) ],[-1.5+Bymove(i)
1.5+Bymove(i) ],'b','linewidth',3);
plot([Axmove(i) Bxmove(i)] , [Aymove(i)
Bymove(i)],'g','linewidth',3);
axis([-10 30 -5 15])
pause(0.05)
%hold off
% plot([O(1),O(2);Axmove(i),Aymove(i)])
% plot(Axmove(i),Aymove(i))
% plot(Bxmove(i),Bymove(i))

end
%% FORCE ANALYSIS
% known vector
b=[0 0 0 0 0 0 1 0 0]' ;
% the unknow vector contains the equilibrium forces in the
following order:
% F1 F2 F3 F4 F5 F6 F7 T8 T
% MATRIX GENERATION
```

```
ics=[];

for i=1:num
    A=[1 0 1 0 0 0 0 0 0 ;
       0 1 0 1 0 0 0 0 0 ;
       0 0 -Aymove(i) Axmove(i) 0 0 0 0 1;
       0 0 -1 0 1 0 0 0 0 ;
       0 0 0 -1 0 1 0 0 0 ;
       0 0 0 0 (Aymove(i) - Bymove(i)) (Bxmove(i)-Axmove(i)) 0 0
0 ;
       0 0 0 0 -1 0 0 0 0 ;
       0 0 0 0 0 -1 1 0 0 ;
       0 0 0 0 0 0 0 1 0 ];
    x=A\b;
    ics=[ics x];
end

T=ics(9,:);
figure
tempo= linspace (0,timereq,100);

subplot(2,2,1)
plot(tempo,radtodeg(TETTA),'r','LineWidth',1.5)
xlabel('time [sec]')
ylabel('\lambda [deg]', 'FontWeight','bold')
%title('position analysis', 'FontWeight','bold')
grid on
subplot(2,2,2)
plot(tempo,radtodeg(PHI),'g','LineWidth',1.5)
xlabel('time [sec]')
ylabel(' \delta [deg]', 'FontWeight','bold')
grid on
subplot(2,2,3)
plot(tempo,(B(1)-SRANGE),'LineWidth',1.5)
xlabel('time [sec]')
ylabel('s [mm]', 'FontWeight','bold')
grid on
subplot(2,2,4)
plot(tempo,-T,'k','LineWidth',1.5)
xlabel('time [sec]')
ylabel('\Gamma [mNm/N]', 'FontWeight','bold')
%title('position analysis', 'FontWeight','bold')
grid on
%%
LAMBDA=TETTA-TETTA(1);
%regression function at varying the retracting lever angle
%LAMBDA=radtodeg(LAMBDA);
[mechadv] = fit( LAMBDA', -T', 'poly3');
regres=mechadv.p1*LAMBDA.^3 + mechadv.p2.*LAMBDA.^2 +
mechadv.p3*LAMBDA+mechadv.p4;
```

```
figure
plot(LAMBDA,-T,'ko','LineWidth',1,'markersize',5)
hold on
plot(LAMBDA,regres,'r','LineWidth',1.5)
%% weight support modeling

distance=linspace(0.0200,0.0400,5);
k=1;
%attraction forces function of distance. offset: remove the
structure weight
ANCHORING =  k*(66.92*exp(-153.5.*distance)+ 12.15*exp(-
52.87.*distance))-0.3215;
LMA =  k*(15.23*exp(-96.2.*distance)+ 0.08597*exp(-
8.989.*distance))-0.2553;
%geometric parameters
c=linspace(0.02,0.05,7);
b=0.05625;%0.0678;
a=0.05625; % 0.052;
TEST=importdata('datiteststatico.txt');

for i=1:5
    for j=1:7
%supported force at different distances
F(i,j)=(ANCHORING(i)*c(j)+LMA(i)*(c(j)+b+a))/(c(j)+a)*1000/9.806
65;
LIFTED(i,j)=TEST((i-1)*7+j,1);
SD(i,j)=TEST((i-1)*7+j,2);
%righa: stessa distanza, colonna: stesso braccio "C"
error(i,j)=(F(i,j)-LIFTED(i,j))/F(i,j)*100;

    end
end

F;
LIFTED;
error
mean(mean(error))
maybe=[];
figure

maybe(1)=plot(c,F(1,:),'k-.','LineWidth',1.5);hold on;
axis([1.8  6.7  0  650])
errorbar(c,LIFTED(1,:),SD(1,:),'b.','LineWidth',1.3)
maybe(2)=plot(c,F(2,:),'k-.','LineWidth',1.5);
errorbar(c,LIFTED(2,:),SD(2,:),'b.','LineWidth',1.3)
%plot(c,LIFTED(2,:),'ro','LineWidth',1.5)
maybe(3)=plot(c,F(3,:),'k-.','LineWidth',1.5);
errorbar(c,LIFTED(3,:),SD(3,:),'b.','LineWidth',1.3)
%plot(c,LIFTED(3,:),'ro','LineWidth',1.5)
```

```
maybe(4)=plot(c,F(4,:),'k-.','LineWidth',1.5);
errorbar(c,LIFTED(4,:),SD(4,:),'b.','LineWidth',1.3)
%plot(c,LIFTED(4,:),'ro','LineWidth',1.5)
maybe(5)=plot(c,F(5,:),'k-.','LineWidth',1.5);
errorbar(c,LIFTED(5,:),SD(5,:),'b.','LineWidth',1.3)
%plot(c,LIFTED(5,:),'ro','LineWidth',1.5)
xlabel('AB lenght [cm]', 'FontWeight','bold')
ylabel('Retracted weight [gr]', 'FontWeight','bold')
title('Structural model validation', 'FontWeight','bold')
%legend([maybe],'@ 2 cm','@ 2.5 cm','@ 3 cm','@ 3.5 cm',' @ 4
cm','Location','EastOutside')
% surf(F); hold on;
% surf(LIFTED)
```